

# 1 **Diastolic dysfunction in prediabetes: role of mitochondrial oxidative stress**

2 **Running head:** Myocardial dysfunction in prediabetes

3

## 4 **Authors**

5 Gábor Koncsos<sup>1\*</sup>, Zoltán V. Varga<sup>1,13\*</sup>, Tamás Baranyai<sup>1</sup>, Kerstin Boengler<sup>2</sup>, Susanne  
6 Rohrbach<sup>2</sup>, Ling Li<sup>2</sup>, Klaus-Dieter Schlüter<sup>2</sup>, Rolf Schreckenber<sup>2</sup>, Tamás Radovits<sup>3</sup>, Attila  
7 Oláh<sup>3</sup>, Csaba Mátyás<sup>3</sup>, Árpád Lux<sup>3</sup>, Tímea Komlódi<sup>4</sup>, Mahmoud Al-Khrasani<sup>1</sup>, Nóra  
8 Bukosza<sup>5</sup>, Domokos Máthé<sup>6,7</sup>, László Deres<sup>8</sup>, Monika Barteková<sup>9,10</sup>, Tomáš Rajtík<sup>11</sup>, Adriana  
9 Adameová<sup>11</sup>, Krisztián Szigeti<sup>6</sup>, Péter Hamar<sup>5</sup>, Zsuzsanna Helyes<sup>12</sup>, László Tretter<sup>4</sup>, Pál  
10 Pacher<sup>1,13</sup>, Béla Merkely<sup>3</sup>, Zoltán Giricz<sup>1†</sup>, Rainer Schulz<sup>2†</sup>, Péter Ferdinandy<sup>1†</sup>

11 <sup>\*,†</sup>Authors contributed equally to this work.

## 12 **Affiliation**

13 <sup>1</sup>Department of Pharmacology and Pharmacotherapy, Faculty of Medicine, Semmelweis University,  
14 Budapest, Hungary

15 <sup>2</sup>Institute of Physiology, Faculty of Medicine, Justus-Liebig University, Giessen, Germany

16 <sup>3</sup>Heart and Vascular Center, Semmelweis University, Budapest, Hungary

17 <sup>4</sup>Department of Medical Biochemistry, Faculty of Medicine, Semmelweis University, Budapest,  
18 Hungary

19 <sup>5</sup>Institute of Pathophysiology, Faculty of Medicine, Semmelweis University, Budapest, Hungary

20 <sup>6</sup>Department of Biophysics and Radiation Biology, Faculty of Medicine, Semmelweis University,  
21 Budapest, Hungary

22 <sup>7</sup>CROmed Translational Research Centers, Budapest, Hungary

23 <sup>8</sup>1st Department of Internal Medicine, Faculty of Medicine, University of Pécs, Pécs, Hungary

24 <sup>9</sup>Institute of Physiology, Faculty of Medicine, Comenius University in Bratislava, Slovakia

25 <sup>10</sup>Institute for Heart Research, Slovak Academy of Sciences, Bratislava, Slovakia

26 <sup>11</sup>Department of Pharmacology and Toxicology, Faculty of Pharmacy, Comenius University in  
27 Bratislava, Slovakia

28 <sup>12</sup>Department of Pharmacology and Pharmacotherapy, Faculty of Medicine and Szentágothai Research  
29 Centre & MTA-PTE NAP B Chronic Pain Research Group, University of Pécs, Pécs, Hungary

30 <sup>13</sup>Laboratory of Cardiovascular Physiology and Tissue Injury, National Institute on Alcohol Abuse and  
31 Alcoholism, National Institutes of Health, Bethesda, Maryland, USA

32 **Address for correspondence**

33 Zoltán Giricz, PharmD, PhD

34 H-1089 Budapest, Nagyvárad tér 4. Hungary

35 Tel.: +36 1 2104416

36 Email: giricz.zoltan@med.semmelweis-univ.hu

37

**39 1. Abstract:**

40 Although incidence and prevalence of prediabetes are increasing, little is known on its cardiac  
41 effects. Therefore, our aim was to investigate the effect of prediabetes on cardiac function and  
42 to characterize parameters and pathways associated with deteriorated cardiac performance.  
43 Long-Evans rats were fed with either control or high-fat chow for 21 weeks and treated with a  
44 single low dose (20 mg/kg) streptozotocin at week 4. High-fat and streptozotocin treatment  
45 induced prediabetes as characterized by slightly elevated fasting blood glucose, impaired  
46 glucose- and insulin tolerance, increased visceral adipose tissue and plasma leptin levels, as  
47 well as sensory neuropathy. In prediabetic animals a mild diastolic dysfunction was observed,  
48 the number of myocardial lipid droplets increased, and left ventricular mass and wall  
49 thickness were elevated, however, no molecular sign of fibrosis or cardiac hypertrophy was  
50 evidenced. In prediabetes, production of reactive oxygen species was elevated in  
51 subsarcolemmal mitochondria. Expression of mitofusin-2 was increased while the  
52 phosphorylation of phospholamban and expression of Bcl-2/adenovirus E1B 19 kDa protein-  
53 interacting protein 3 (BNIP3, a marker of mitophagy) decreased. However, expression of  
54 other markers of cardiac auto- and mitophagy, mitochondrial dynamics, inflammation, heat  
55 shock proteins, Ca<sup>2+</sup>/calmodulin-dependent protein kinase II, mTOR or apoptotic pathways  
56 were unchanged in prediabetes. This is the first comprehensive analysis of cardiac effects of  
57 prediabetes indicating that mild diastolic dysfunction and cardiac hypertrophy are  
58 multifactorial phenomena which is associated with early changes in mitophagy, cardiac lipid  
59 accumulation and elevated oxidative stress, and that prediabetes-induced oxidative stress  
60 originates from the subsarcolemmal mitochondria.

61 **Keywords:** obesity, type 2 diabetes, high-fat diet, ROS, diabetic cardiomyopathy

63

64 **New and Noteworthy**

65 In prediabetes induced by chronic high-fat diet and a low single dose of streptozotocin in rats,  
66 mild diastolic dysfunction and ventricular hypertrophy are observed. Elevated cardiac lipid  
67 accumulation, subsarcolemmal mitochondrial reactive oxygen species production, and early  
68 changes in cardiac mitophagy may be responsible for cardiac effects of prediabetes.

## 70 **1. Introduction:**

71 Type 2 diabetes mellitus is a common civilization disease with a growing prevalence  
72 worldwide (1, 66, 79). It is well established that type 2 diabetes mellitus is a risk factor of  
73 cardiovascular diseases such as heart failure and myocardial infarction contributing to their  
74 increased morbidity and mortality (6, 66). However, before the development of overt diabetes,  
75 a period of prediabetic state (*i.e.*, impaired glucose and insulin tolerance, insulin and leptin  
76 resistance, oscillations of normo- and hyperglycemic states, mild to moderate obesity) occurs  
77 (54), which may also promote cardiovascular complications (21, 30, 45). Although cardiac  
78 pathophysiological alterations are relatively well characterized in fully developed diabetes  
79 (*i.e.*, diabetic cardiomyopathy), information about prediabetes is quite limited. It has been  
80 reported that prediabetes induced mild diastolic dysfunction in OLETF rats, which is a genetic  
81 model for spontaneous long-term hyperglycemia (51), however, cardiac consequences of  
82 prediabetes and their molecular mechanism is unknown in non-genetic prediabetic settings.

83 Contractile dysfunction in diabetic cardiomyopathy has been attributed to numerous factors  
84 and pathways (*i.e.*, increased oxidative stress, or activated apoptosis (13, 76), of which could  
85 be connected to an impaired mitochondrial function (24), autophagy (41, 76) or to an  
86 imbalance in the calcium homeostasis (59)). Although these pathways are well studied in  
87 diabetes, their role in prediabetes has not been uncovered. Furthermore, since mitochondrial  
88 function is heavily influenced by mitochondrial dynamics including mitochondrial biogenesis,  
89 fusion, fission, and autophagy-mitophagy, and since these processes have been linked to the  
90 development of diabetic cardiomyopathy (13, 32, 41, 76), we hypothesized that altered  
91 mitochondrial dynamics might be involved in the mechanism of deteriorated cardiac functions

92 in prediabetes. Moreover, development of diabetes leads to systemic sensory neuropathy that  
93 has been shown to result in diastolic dysfunction in the rat heart (7, 84).  
94 Therefore, here we aimed to systematically characterize the cardiac effect of prediabetes on  
95 functional, morphological and molecular levels in a non-genetic rodent model.

## 97 **2. Materials and Methods:**

98 This investigation conforms to the Guide for the Care and Use of Laboratory Animals  
99 published by the US National Institutes of Health (NIH publication No. 85–23, revised 1996)  
100 and was approved by the animal ethics committee of the Semmelweis University, Budapest,  
101 Hungary (registration numbers: XIV-I-001/450-6/2012). Chemicals were purchased from  
102 Sigma, St. Louis, MO unless otherwise noted.

### 103 **Animal model and experimental design**

104 Male Long-Evans rats of 5-7 weeks of age were purchased from Charles River Laboratories  
105 (Wilmington, MA). Animals were housed in a room maintained at 12 h light-dark cycles and  
106 constant temperature of 21°C. Animals were allowed to food and water *ad libitum*. After one  
107 week of acclimatization rats were divided into two groups: control (CON; n=20) and  
108 prediabetic group (PRED; n=20) (Fig. 1). The control group was fed control chow, while the  
109 prediabetic group was fed a chow supplemented with 40% lard as a high-fat diet. Body  
110 weights were measured weekly. Blood was taken and fasting blood glucose levels were  
111 measured from the saphenous vein every second week with a blood glucose monitoring  
112 system (Accu-Check, Roche, Basel, Switzerland). To facilitate the development of  
113 prediabetes and to avoid hypoinsulinemia, animals on high-fat diet received 20 mg/kg  
114 streptozotocin (STZ, Santa Cruz Biotechnology, Dallas, TX) intraperitoneally (i.p.) at the  
115 fourth week of the diet according to Mansor *et al.* (50), while the control group was treated  
116 with same volume of ice-cold citrate buffer as vehicle. At the 20<sup>th</sup> week oral glucose tolerance  
117 test (OGTT) was performed in overnight fasted rats with *per os* administration of 1.5 g/kg  
118 glucose and measurements of plasma glucose levels at 15, 30, 60 and 120 minutes. Insulin  
119 tolerance test (ITT) was also performed at week 20 in overnight fasted rats. Insulin (0.5

120 IU/kg, Humulin R, Ely Lilly, Netherlands) was injected i.p. and plasma glucose levels were  
121 checked at 15, 30, 45, 60, 90 and 120 minutes. At week 21 of the diet, animals were  
122 anesthetized with pentobarbital (60 mg/kg, i.p., Euthasol, Produlab Pharma, Raamsdonksveer,  
123 Netherlands). Echocardiography and cardiac catheterization were performed, then hearts were  
124 excised, shortly perfused with oxygenated Krebs-Henseleit buffer in Langendorff mode as  
125 described earlier and heart weights were measured. Epididymal and interscapular brown fat  
126 tissue, which are the markers of adiposity (9, 34), were isolated and their weights were  
127 measured. Blood and tissue samples were collected and stored at -80°C.

#### 128 **Assesment of sensory neuropathy**

129 To test if sensory neuropathy develops in prediabetes, plantar Von Frey test was performed.  
130 At week 15 of the diet, rats were placed in a plastic cage having a wire mesh bottom to allow  
131 full access to the paws. After 5-10 min acclimation time, mechanical hind paw withdrawal  
132 thresholds were measured by a dynamic plantar aesthesiometer (UGO-Basile, Monvalle,  
133 Italy) as previously described (55).

#### 134 **Evaluation of body fat content**

135 At week 20 of the diet, computer tomography (CT) measurements were performed on  
136 NanoSPECT/CT PLUS (Mediso, Budapest, Hungary). The semicircular CT scanning was  
137 acquired with 55 kV tube voltage, 500 ms of exposure time, 1:4 binning and 360 projections  
138 in 18 minutes 7s. During the acquisitions, rats were placed in prone position in a dedicated rat  
139 bed, and were anesthetized with 2% isoflurane in oxygen. Temperature of the animals was  
140 kept at  $37.2\pm 0.3^{\circ}\text{C}$  during imaging. In the reconstruction, 0.24 mm in-plane resolution and  
141 slice thickness were set and Butterworth filter was applied (volume size: 76.8\*76.8\*190 mm).  
142 Images were further analyzed with VivoQuant (inviCRO LLC) dedicated image analysis  
143 software products by placing appropriate Volume-of-Interests (VOI) on the whole body fat of

144 animals. The aim of segmentation was to separate the fat from other tissues. The connected  
145 threshold method helped to choose the adequate attenuated pixels for fat tissue analysis, then  
146 the isolated points were detected by erode 4 voxel and dilate 4 voxel steps. After the  
147 measurements animals recovered from anesthesia.

#### 148 **Cardiac function by echocardiography**

149 Before euthanasia, to measure cardiac function, echocardiography was performed as  
150 previously described (42, 62). Briefly, anesthetized animals were placed on a controlled  
151 heating pad, and the core temperature, measured via rectal probe, was maintained at 37°C.  
152 Transthoracic echocardiography was performed in supine position by one investigator blinded  
153 to the experimental groups. Two dimensional and M-mode echocardiographic images of long  
154 and short (mid-papillary muscle level) axis were recorded, using a 13 MHz linear transducer  
155 (GE 12L-RS, GE Healthcare), connected to an echocardiographic imaging unit (Vivid i, GE  
156 Healthcare). The digital images were analyzed by a blinded investigator using an image  
157 analysis software (EchoPac, GE Healthcare). On two dimensional recordings of the short-axis  
158 at the mid-papillary level, left ventricular (LV) anterior (LVAWT) and posterior (LVPWT)  
159 wall thickness in diastole (index: d) and systole (index: s), left ventricular end-diastolic  
160 (LVEDD) and end-systolic diameter (LVESD) were measured. In addition, end-diastolic and  
161 end-systolic LV areas were planimetered from short and long axis two dimensional  
162 recordings. End-systole was defined as the time point of minimal left ventricular dimensions,  
163 and end-diastole as the time point of maximal dimensions. All values were averaged over  
164 three consecutive cycles. The following parameters were derived from these measurements  
165 (63). Fractional shortening (FS) was calculated as  $((LVEDD-LVESD)/LVEDD) \times 100$ . LV  
166 mass was calculated according to the following formula:  
167  $[LV_{mass} = (LVEDD + AWTd + PWTd)^3 - LVEDD^3] \times 1.04 \times 0.8 + 0.14$ .

168 **Hemodynamic measurements, left ventricular pressure-volume analysis**

169 After echocardiographic measurements, hemodynamic measurement was performed as  
170 previously described (60, 61). Briefly, rats were tracheotomized, intubated and ventilated,  
171 while core temperature was maintained at 37°C. A median laparotomy was performed. A  
172 polyethylene catheter was inserted into the left external jugular vein. A 2-Fr microtip  
173 pressure-conductance catheter (SPR-838, Millar Instruments, Houston, TX) was inserted into  
174 the right carotid artery and advanced into the ascending aorta. After stabilization for 5 min,  
175 mean arterial blood pressure (MAP) was recorded. After that, the catheter was advanced into  
176 the LV under pressure control. After stabilization for 5 min, signals were continuously  
177 recorded at a sampling rate of 1,000/s using a Pressure-Volume (P-V) conductance system  
178 (MPVS-Ultra, Millar Instruments, Houston, TX) connected to the PowerLab 16/30 data  
179 acquisition system (AD Instruments, Colorado Springs, CO), stored and displayed on a  
180 personal computer by the LabChart5 Software System (AD Instruments). After positioning  
181 the catheter baseline P-V loops were registered. With the use of a special P-V analysis  
182 program (PVAN, Millar Instruments), LV end-systolic pressure (LVESP), LV end-diastolic  
183 pressure (LVEDP), the maximal slope of LV systolic pressure increment ( $dp/dt_{max}$ ) and  
184 diastolic pressure decrement ( $dp/dt_{min}$ ), time constant of LV pressure decay ( $\tau$ ; according to  
185 the Glantz method), ejection fraction (EF) stroke work (SW) and LV maximal power were  
186 computed and calculated. Stroke volume (SV) and cardiac output (CO) were calculated and  
187 corrected according to in vitro and in vivo volume calibrations using the PVAN software.  
188 Total peripheral resistance (TPR) was calculated by the following equation:  $TPR=MAP/CO$ .  
189 In addition to the above parameters, P-V loops recorded at different preloads can be used to  
190 derive other useful systolic function indexes that are less influenced by loading conditions and  
191 cardiac mass (37, 57). Therefore, LV P-V relations were measured by transiently compressing  
192 the inferior vena cava (reducing preload) under the diaphragm with a cotton-tipped applicator.

193 The slope of the LV end-systolic P-V relationship (ESPVR; according to the parabolic  
194 curvilinear model), preload recruitable stroke work (PRSW), and the slope of the  $dp/dt_{max}$  -  
195 end-diastolic volume relationship ( $dp/dt_{max}$ -EDV) were calculated as load-independent  
196 indexes of LV contractility. The slope of the LV end-diastolic P-V relationship (EDPVR) was  
197 calculated as a reliable index of LV stiffness (37). At the end of each experiment, 100  $\mu$ L of  
198 hypertonic saline were injected intravenously, and from the shift of P-V relations, parallel  
199 conductance volume was calculated by the software and used for the correction of the cardiac  
200 mass volume. The volume calibration of the conductance system was performed as previously  
201 described (37).

#### 202 **Adipokine array from rat plasma**

203 Adipokine array was performed from 1 mL rat plasma according to manufacturer's  
204 instructions (Proteome Profiler Rat Adipokine Array Kit, R&D Systems, Abingdon, UK).

#### 205 **Biochemical measurements**

206 Serum cholesterol, high density lipoprotein (HDL) and triglyceride levels were measured by  
207 colorimetric assays (Diagnosticum, Budapest, Hungary) as previously described (19). Plasma  
208 leptin (Invitrogen, Camarillo, CA), TIMP metalloproteinase inhibitor 1 (TIMP-1; R&D  
209 System, Minneapolis, MN) and angiotensin-II (Phoenix pharmaceuticals, Karlsruhe,  
210 Germany) were measured by enzyme-linked immunosorbent assay (ELISA) according to  
211 manufacturer's instructions. Urea, glutamate oxaloacetate transaminase (GOT), glutamate  
212 pyruvate transaminase (GPT), low density lipoprotein (LDL), C-reactive protein (CRP),  
213 cholesterol, uric acid and creatinine were measured by automated clinical laboratory assays  
214 (Diagnosticum, Budapest, Hungary).

#### 215 **Histology**

216 Heart, liver and pancreas samples were fixed in 4% neutral-buffered formalin. After 24 hours,  
217 samples were washed with phosphate buffered saline (PBS) and stored in 70% ethanol in PBS  
218 until embedded in paraffin. Samples were stained with hematoxylin-eosin (HE) and Masson's  
219 trichrome (MA) staining. Left ventricle samples were analyzed to examine histopathological  
220 differences and evaluate cardiomyocyte hypertrophy and fibrosis. The level of fibrosis was  
221 measured on MA-stained LV sections, and transverse transnuclear width (cardiomyocyte  
222 diameter) was assessed on longitudinally oriented cardiomyocytes on HE-stained LV sections  
223 by a Zeiss microscope (Carl Zeiss, Jena, Germany). Digital images were acquired using an  
224 imaging software (QCapture Pro 6.0, QImaging, Canada) at 20× magnification.  
225 Quantification of cardiomyocyte diameter and fibrosis was performed with ImageJ Software  
226 (v1.48, NIH, Bethesda). Liver samples were evaluated for hepatic steatosis/fibrosis and scored  
227 as previously described (40).

#### 228 **Nitrotyrosine immunostaining of left ventricular samples**

229 After embedding and cutting 5 µm thick sections, heat-induced antigen epitope retrieval was  
230 performed (95°C, 10 min, in citrate buffer with a pH of 6.0). Sections were stained with  
231 rabbit polyclonal anti-nitrotyrosine antibody (5 µg/mL, Cayman Chemical, Ann Arbor, MI)  
232 by using the ABC-kit of Vector Laboratories (Burlingame, CA) according to the  
233 manufacturer's protocol. Nitrotyrosine-stained sections were counterstained with  
234 hematoxylin. Specific staining was visualized and images were acquired using a BX-41  
235 microscope (Olympus, Tokyo, Japan).

236

#### 237 **Quantitative RT-PCR**

238 Total RNA was isolated from LV tissue with RNeasy<sup>TM</sup> RNA Tissue Miniprep kit  
239 (Qiagen, Madison, WI) according to the manufacturer's instructions. cDNA was  
240 synthesized using Tetro cDNA Synthesis Kit (Bioline, London, UK) according to the

241 manufacturer's protocol. PCR reaction was performed with iQ SYBR Green Supermix (Bio-  
242 Rad, Hercules, CA), or TaqMan Universal PCR MasterMix (Thermo Fisher Scientific,  
243 Waltham, MA) and 3 nM forward and reverse primers for collagen type 1 and 3 (COL1 and  
244 COL3), atrial natriuretic peptide (ANP), brain natriuretic peptide (BNP) (Integrated DNA  
245 Technologies, Leuven, Belgium), assay mixes for  $\alpha$ -myosin heavy chain ( $\alpha$ -MHC, assay ID:  
246 Rn00691721\_g1),  $\beta$ -myosin heavy chain ( $\beta$ -MHC, assay ID: Rn00568328\_m1), tumor  
247 necrosis factor  $\alpha$  (TNF- $\alpha$ , assay ID: Rn99999017\_m1) and interleukin-6 (IL-6, assay ID:  
248 Rn01410330\_m1, Thermo Fisher Scientific, Waltham, MA) were used. Beta-2  
249 microglobulin (B2M) or glyceraldehyde-3-phosphate dehydrogenase (GAPDH; reference  
250 gene; assay ID: Rn01775763\_g1) were used as reference genes. Quantitative real-time PCR  
251 was performed with the StepOnePlus Real-Time PCR System (Thermo Fisher Scientific,  
252 Waltham, MA). Expression levels were calculated using the CT comparative method ( $2^{-\Delta CT}$ ).

253

#### 254 **Measurement of pancreatic insulin**

255 Freeze clamped and pulverized pancreas samples were used to determine pancreatic insulin  
256 content. Analysis was performed with Insulin (I-125) IRMA Kit (Izotop Kft, Budapest,  
257 Hungary) according to the manufacturer's instructions.

#### 258 **Electron microscopy**

259 Left ventricular tissue samples (1×1 mm) were placed in modified Kranovsky fixative (2%  
260 paraformaldehyde, 2.5 % glutaraldehyde, 0.1 M Na-cacodylate buffer, pH 7.4 and 3mM  
261 CaCl<sub>2</sub>). After washing in cacodylate buffer, samples were incubated in 1% osmium tetroxide  
262 in 0.1 M PBS for 35 min. Then samples were washed in buffer several times for 10 minutes  
263 and dehydrated in an ascending ethanol series, including a step of uranyl acetate (1%) solution  
264 in 70% ethanol to increase contrast. Dehydrated blocks were transferred to propylene oxide

265 before being placed into Durcupan resin. Blocks were placed in thermostat for 48 h at 56 °C.  
266 From the embedded blocks, 1 µm-thick semithin and serial ultrathin sections (70 nm) were  
267 cut with a Leica ultramicrotome, and mounted either on mesh, or on Collodion-coated  
268 (Parlodion, Electron Microscopy Sciences, Fort Washington, PA) single-slot copper grids.  
269 Additional contrast was provided to these sections with uranyl acetate and lead citrate  
270 solutions, and they were examined with a JEOL1200EX-II electron microscope. Areas of  
271 subsarcolemmal (SSM), interfibrillar mitochondria (IFM) and lipid droplets were measured  
272 by free hand polygon selection in iTEM Imaging Platform.

### 273 **Mitochondrial enzyme activity measurements**

274 Fresh myocardial samples were homogenized in 1/30 weight per volume Chappel-Perry  
275 buffer (100 mM KCl, 5 mM MgCl<sub>2</sub>, 1 mM EDTA, 50 mM Tris, pH: 7.5) supplemented with  
276 15 mg/L trypsin-inhibitor, 15.5 mg/L benzamidine, 5 mg/L leupeptin and 7 mg/L pepstatin  
277 A. All enzyme activities were measured as duplicates with a photometer (Cary 50 Scan UV-  
278 Visible Spectrophotometer, Varian). Before adding substrate or cofactor, the reaction mix was  
279 incubated at 30°C for 10 min (except for cytochrome c oxidase). Enzyme activities were  
280 expressed relative to citrate synthase activity or total protein levels (measured with  
281 Bicinchoninic Acid assay). The activity of rotenone-sensitive NADH:ubiquinone-  
282 oxidoreductase (Complex I) was measured at 340 nm in the presence of 1 mM EDTA, 2.5  
283 mM KCN, 1 µM antimycin A and 20 µM rotenone after adding coenzyme Q and NADH to a  
284 final concentration of 60 µM. The activity of NADH:cytochrome c-oxidoreductase (Complex  
285 I+III) was measured at 550 nm as the antimycin A- and rotenone-sensitive fraction of total  
286 NADH-cytochrome c oxidoreductase in the presence of 0.1 mM EDTA, 3 mM KCN and  
287 0.1% cytochrome c after adding NADH to a final concentration of 0.2 mM. The activity of  
288 succinate:cytochrome c-oxidoreductase (Complex II+III) was measured at 550 nm in the  
289 presence of 0.1 mM EDTA, 2.5 mM KCN, 0.1% bovine serum albumin and 4 mM succinate

290 after adding cytochrome c to a final concentration of 0.1%. The activity of succinate-  
291 dehydrogenase was measured at 600 nm in the presence of 0.1 mM EDTA, 2.5 mM KCN,  
292 0.1% bovine serum albumin and 2 mM succinate after adding 2,6-dichloroindophenol and  
293 phenazine-methosulfate to a final concentration of 34.9  $\mu$ M and 1.625 mM, respectively. The  
294 activity of cytochrome c-oxidase was measured at 550 nm in the presence of 0.08% reduced  
295 cytochrome c. The activity of citrate-synthase was measured at 412 nm in the presence of  
296 0.1% triton-X 100, 0.1 mM 5,5'-dithiobis (2-nitrobenzoic acid), and 0.1 mM acetyl-coenzyme  
297 A after adding oxalacetate to a final concentration of 0.5 mM.

### 298 **Preparation of isolated mitochondria**

299 SSM and IFM fractions were isolated according to a protocol described previously (72).  
300 Using homogenization buffer (buffer A) containing (mM): 100 KCl, 50 MOPS, 5 MgSO<sub>4</sub>, 1  
301 EGTA and pH 7.4 (Tris-HCl). Isolation buffer (buffer B) containing (mM): 250 sucrose, 10  
302 HEPES, 1 EGTA and pH 7.4 (Tris-HCl). Before the isolation, 1 mM ATP was added freshly  
303 to the homogenization buffer. All steps were carried out on ice. After Langendorff perfusion  
304 of the heart LV samples were cut to small species with scissors and washed in buffer A, then  
305 homogenized with five strokes of teflon pistils in a glass potter. The homogenate was  
306 centrifuged for 10 min at 800 $\times$ g, 4°C. For isolation of SSM the supernatant was centrifuged  
307 for 10 min at 8,000 $\times$ g. This pellet was suspended in buffer A and centrifuged for 10 min at  
308 8,000 $\times$ g, and the resulting sediment was resuspended in a small volume of buffer A. The  
309 pellet of the first centrifugation was used for isolation of IFM fraction and resuspended in  
310 buffer B (10 mL/g tissue) and after addition of 8 U/g of bacterial protease incubated for 1 min  
311 on ice and then homogenized with five strokes of teflon pistil in a glass potter and centrifuged  
312 for 10 min at 800 $\times$ g. The supernatant was centrifuged for 10 min at 8,000 $\times$ g, the resulting  
313 mitochondrial pellet was finally resuspended in buffer A and used for mitochondrial  
314 respiration, membrane potential, H<sub>2</sub>O<sub>2</sub> production and Ca<sup>2+</sup> uptake measurements. For

315 Western blots, the resulting SSM and IFM pellets were finally resuspended in 200  $\mu$ L volume  
316 of Buffer B which were layered on 30% Percoll Solution and were ultracentrifuged (Rotor  
317 type: Beckman Type 70.1 Ti) for 30 min at 18,700 $\times$ g at 4°C. After ultracentrifugation, lower  
318 rings were collected (100  $\mu$ L/ tube) and filled with 1 mL Buffer B and centrifuged for 10 min  
319 at 12,200 $\times$ g, 4°C. After washing, pellets were stored at -80°C.

### 320 **Measurement of mitochondrial respiration**

321 Protein concentration of SSM and IFM samples was determined by biuret method (11).  
322 Mitochondrial oxygen consumption was measured by high-resolution respirometry with  
323 Oxygraph-2K (Oroboros Instruments, Innsbruck, Austria) a Clark-type O<sub>2</sub> electrode for 40  
324 min. The mitochondrial protein content was 0.1 mg/mL in the measurements. Measuring  
325 mitochondrial respiration followed the substrate-uncoupler-inhibitor titration (SUIT) protocol.  
326 Mitochondria were energized with 5 mM glutamate and 5 mM malate. Mitochondrial  
327 respiration was initiated with 2 mM adenosine diphosphate (ADP). Cytochrome c (4  $\mu$ M),  
328 succinate (5 mM), rotenone (1  $\mu$ M) and carboxyatractyloside (CAT; 2  $\mu$ M) were used as  
329 indicated. Measurements were performed in an assay medium containing 125 mM KCl, 20  
330 mM HEPES, 100  $\mu$ M EGTA, 2 mM K<sub>2</sub>HPO<sub>4</sub>, 1 mM MgCl<sub>2</sub> and 0.025% BSA. Data were  
331 digitally recorded using DatLab4 software.

### 332 **Measurement of mitochondrial membrane potential**

333 To detect mitochondrial membrane potential, we used the fluorescent, cationic dye, safranin  
334 O (2  $\mu$ M) which can bind to the protein possessing negative charge in the inner mitochondrial  
335 membrane depending on the mitochondrial membrane potential. The excitation/emission  
336 wavelengths were 495/585 nm. Fluorescence was recorded at 37°C by Hitachi F-4500  
337 spectrofluorimeter (Hitachi High Technologies, Maidenhead, UK). The reaction medium was

338 the following: 125 mM KCl, 20 mM HEPES, 100  $\mu$ M EGTA, 2 mM K<sub>2</sub>HPO<sub>4</sub>, 1 mM MgCl<sub>2</sub>  
339 and 0.025% BSA.

#### 340 **Detection of H<sub>2</sub>O<sub>2</sub> formation in mitochondria**

341 H<sub>2</sub>O<sub>2</sub> production of SSM and IFM was assessed by Amplex UltraRed fluorescent dye method  
342 (52). Horseradish peroxidase (2.5 U/mL) and Amplex UltraRed reagent (1  $\mu$ M), then 0.05  
343 mg/mL mitochondria were added to the incubation medium. H<sub>2</sub>O<sub>2</sub> formation was initiated by  
344 the addition of 5 mM glutamate and 5 mM malate or 5 mM succinate and fluorescence was  
345 detected at 37°C with Deltascan fluorescence spectrophotometer (Photon Technology  
346 International, PTI, Lawrenceville, NJ). The excitation wavelength was 550 nm and the  
347 fluorescence emission was detected at 585 nm. A calibration signal was generated with  
348 known quantities of H<sub>2</sub>O<sub>2</sub> at the end of each experiment.

#### 349 **Measurement of Ca<sup>2+</sup> - uptake in mitochondria**

350 The free Ca<sup>2+</sup> concentration at each added concentration of Ca<sup>2+</sup> was calculated and measured.  
351 Ca<sup>2+</sup> uptake by mitochondria was followed by measuring Calcium-Green-5N (100 nM)  
352 fluorescence at 505 nm excitation and 535 emission wavelengths at 37°C using a Hitachi F-  
353 4500 spectrofluorimeter (Hitachi High Technologies, Maidenhead, UK). The reaction  
354 medium was the following: 125 mM KCl, 20 mM HEPES, 100  $\mu$ M EGTA, 2 mM K<sub>2</sub>HPO<sub>4</sub>, 1  
355 mM MgCl<sub>2</sub> and 0.025% BSA.

#### 356 **Western blot of left ventricle lysates and isolated mitochondria fractions**

357 Freeze clamped left ventricles were pulverized under liquid nitrogen and homogenized in  
358 homogenization buffer containing (in mmol/L): 20 Tris-HCl, 250 sucrose, 1.0 EGTA, 1.0  
359 dithiothreitol, or in radioimmunoprecipitation assay buffer (Cell Signaling Technology,  
360 Danvers, MA), supplemented with 1 mM phenylmethylsulphonylfluoride (PMSF; Roche,

361 Basel, Switzerland), 0.1 mM sodium fluoride, 200mM sodium orthovanadate and complete  
362 protease inhibitor cocktail (Roche, Basel, Switzerland) with TissueLyser LT (Qiagen, Venlo,  
363 Netherlands) to obtain LV soluble protein fraction or LV whole cell lysate. Previously  
364 isolated mitochondrial samples were resuspended in ice-cold 1x cell lysis buffer (Cell  
365 Signaling Technology, Danvers, MA). Concentration of proteins was assessed with Lowry's  
366 assay or Bicinchoninic Acid Assay kit (Thermo Fisher Scientific, Waltham, MA).

367 For tropomyosin oxidation analysis, tissue samples were homogenized in ice-cold PBS, pH  
368 7.2 containing an antiprotease mixture (Complete, Roche, Basel, Switzerland) and 5 mM  
369 EDTA. Just before use, the protein samples were stirred under vacuum and bubbled with  
370 argon to maximally reduce the oxygen tension. The protein suspension was centrifuged at  
371 12,000×g for 10 min at 4°C. The resulting pellet was resuspended in sample buffer (2% SDS,  
372 5% glycerol, 1% β-mercaptoethanol, 125 mM Tris-HCl, pH 6.8) and denatured by 10 min  
373 boiling. This procedure referred to as reducing condition was compared with the non-reducing  
374 condition obtained without the addition of β-mercaptoethanol. To avoid artifacts due to the  
375 oxidation of thiol groups in vitro, non-reducing conditions were performed in the presence of  
376 1 mM N-ethylmaleimide.

377 Protein samples were resolved on precast 4–20% Criterion TGX gels (Bio-Rad, Hercules,  
378 CA) or bis-tris gels depending on the protein of interest and transferred to nitrocellulose or  
379 Immun-Blot PVDF membranes (Bio-Rad, Hercules, CA). Quality of transfer was verified  
380 with Ponceau S staining. Membranes were blocked with 5% nonfat milk (Bio-Rad, Hercules,  
381 CA) or 2-5% bovine serum albumin (BSA; Santa Cruz Biotechnology, Dallas, TX) in Tris-  
382 buffered saline with 0.05% Tween 20 (TBS-T) for 0.5-2 hours. Membranes were incubated  
383 with primary antibodies in 1-5% nonfat milk or BSA in TBS-T: anti-tropomyosin (Tm; 1:250)  
384 anti-phospho-phospholamban (PLB-Ser<sup>16</sup>; 1:5,000), p-PLB (Thr<sup>17</sup>; 1:5,000), anti-  
385 sarco/endoplasmic reticulum Ca<sup>2+</sup>-ATPase II (SERCA2A; 1:5,000, Badrilla, Leeds, UK),

386 anti-heat shock protein-60 (HSP-60; 1:500), anti-HSP-70 (1:500), anti-HSP-90 (1:500), anti-  
387 B-cell lymphoma 2 (Bcl-2; 1:500), anti-caspase-3 (1:500), anti-Ca<sup>2+</sup>/calmodulin-dependent  
388 protein kinase II (CaMKII $\delta$ ; 1:2,000), anti-Parkin (1:5,000, Santa Cruz Biotechnology, Dallas,  
389 TX), anti-Shc (1:1,000), anti-dynamin-related/like protein 1 (DRP1/DLP1; 1:5,000), anti-  
390 optic atrophy 1 protein (OPA1; 1:2,500, BD Biosciences, Franklin Lakes, NJ), anti-mitofusin-  
391 2 (MFN2; 1:2,500, Abcam, Cambridge, UK), anti-phospho-CaMKII $\delta$  (Thr<sup>287</sup>; 1:2,000) anti-  
392 phospho-HSP-27 (Ser<sup>82</sup>; 1:1,000), anti-HSP-27 (1:1,000), anti-Bax (1:1,000), anti-  
393 sequestosome 1 (SQSTM1/p62; 1:1,000), anti-microtubule-associated protein 1 light chain 3  
394 A/B (LC3 A/B; 1:5,000), anti-Beclin-1 (1:1,000), anti-Bcl-2/adenovirus E1B 19 kDa protein-  
395 interacting protein 3 (BNIP3; 1:5,000), anti-phospho-Akt (Ser<sup>473</sup>; 1:1,000), anti-Akt (1:1,000),  
396 anti-phospho-AMP-activated protein kinase  $\alpha$  (AMPK $\alpha$ -Thr<sup>172</sup>; 1:1,000), anti-AMPK $\alpha$   
397 (1:1,000), anti-phospho-ribosomal S6 (Ser<sup>235/236</sup>; 1:1,000), anti-ribosomal S6 (1:1,000), anti-  
398 phospho-glycogen synthase kinase-3 beta (GSK3 $\beta$ -Ser<sup>9</sup>; 1:1,000), anti-GSK3 $\beta$  (1:1,000) and  
399 anti-GAPDH (1:5,000) as loading control (Cell Signaling Technology, Danvers, MA). For  
400 isolated mitochondria the following primary antibodies were used in 5% nonfat milk in TBS-  
401 T: anti-OPA1 (1:2,500) from BD Bioscience (Franklin Lakes, NJ), anti-SQSTM1/p62  
402 (1:1,000), anti-LC3 A/B (1:1,000) and anti-cytochrome c oxidase subunit 4 (COX4; 1:5,000)  
403 as loading control from Cell Signaling Technology (Danvers, MA). After three washes with  
404 TBS-T, horseradish peroxidase conjugated secondary antibody was added for 2 hours at room  
405 temperature (1:5,000 in 5% nonfat milk in TBS-T). Signals were detected with an enhanced  
406 chemiluminescence kit (Bio-Rad, Hercules, CA) by Chemidoc XRS+ (Bio-Rad, Hercules,  
407 CA). For the analysis of tropomyosin oxidation, the density of the additional band with higher  
408 molecular weight reflecting the formation of disulfide crossbridges was normalized to  
409 densitometric values of the respective tropomyosin monomer. Antibodies against

410 phosphorylated epitopes were removed with Pierce Stripping Buffer (Thermo Fisher  
411 Scientific, Waltham, MA) before incubation with antibodies detecting the total protein.

412 **Statistical analysis**

413 Values are expressed as mean±standard error of mean (SEM). Statistical analysis was  
414 performed between groups by unpaired two-tailed T-test or by Mann-Whitney U-test by using  
415 GraphPad Prism 6 software. A  $p < 0.05$  value was considered significant.

416

417

### 418 **3. Results:**

#### 419 **Moderately increased adiposity in prediabetic animals**

420 To determine the effect of high-fat diet and the single, low dose STZ injection, we measured  
421 body weight, fat tissue volumes and plasma lipid parameters. We found that body weights of  
422 the prediabetic animals were moderately but statistically significantly elevated from week 9 as  
423 compared to the control group, and that this difference reached 18% at the end of the diet  
424 period (Fig. 2, *A-B*). At week 20, plasma leptin level was significantly increased in  
425 prediabetes, however, CRP level was decreased, plasma cholesterol, HDL cholesterol and  
426 triglyceride levels, and parameters of liver and kidney function were unchanged (Table 1). To  
427 characterize prediabetes-induced changes in further obesity-related molecules, we performed  
428 an adipokine array measurement, which revealed that the circulating level of tissue inhibitor  
429 of matrix metalloprotease-1 (TIMP-1) might be influenced by prediabetes, however, we could  
430 not confirm these results by ELISA (data not shown). CT scan showed that body fat volume  
431 of prediabetic rats was substantially increased at the end of the diet (Fig. 2, *C-D*). Epididymal  
432 fat tissue weight, which is an indicator of total body adiposity, was increased in the  
433 prediabetic group, however, the weight of interscapular brown adipose tissue was not changed  
434 (Fig. 2, *G-I*). Histological score analysis of HE and MA-stained liver samples evidenced the  
435 development of hepatic steatosis in the prediabetic group (CON:  $0.5 \pm 0.3$  vs. PRED:  $2.25 \pm 0.5$ ;  
436  $p < 0.05$ ), however, no signs of hepatic fibrosis was detected (Fig. 2*H*). Furthermore, electron  
437 microscopy showed an increased number of lipid droplets in the myocardium of prediabetic  
438 animals as compared to controls (Fig. 2, *E-F*). These results demonstrated a moderately  
439 increased adiposity, hepatic and cardiac fat deposits without signs of hyperlipidemia in the  
440 prediabetic group.

441 **Impaired glucose tolerance, insulin resistance, and sensory neuropathy evidence**  
442 **disturbed carbohydrate metabolism in prediabetes**

443 We aimed to characterize the glucose homeostasis in our rat model of prediabetes. At week 20  
444 of the diet, fasting blood glucose levels were slightly elevated in prediabetes from week 10,  
445 however, remained in the normoglycemic range (Fig. 3, A-B). OGTT and ITT demonstrated  
446 impaired glucose tolerance and insulin resistance in the prediabetic group (Fig. 3, C-F),  
447 however, there was no difference in pancreatic insulin content (Fig. 3G), or in pancreatic islet  
448 morphology (data not shown) between groups. These results demonstrate prediabetic  
449 conditions in the present model and evidence that type 1 diabetes did not develop due to the  
450 STZ treatment. Sensory neuropathy is a well-accepted accompanying symptom of diabetes  
451 (78). Accordingly, here we have found a decrease in the mechanical hind limb withdrawal  
452 threshold at week 15 (CON:  $48\pm 1g$  vs. PRED:  $42\pm 2g$ ;  $p<0.05$ ) of diet in the PRED, which  
453 indicates a moderate sensory neuropathy in this model of prediabetes.

454 **Diastolic dysfunction and hypertrophy in prediabetes with no sign of fibrosis**

455 To determine the cardiac effect of prediabetes, we measured morphological and functional  
456 parameters of the hearts. Heart weights were significantly increased (Fig. 4A), however, heart  
457 weight/body weight ratio was decreased in prediabetes (CON:  $0.27\pm 0.01\%$  vs. PRED:  
458  $0.24\pm 0.01\%$ ;  $p<0.05$ ), plausibly due to obesity. Left ventricular (LV) mass, left ventricular  
459 anterior wall thickness, systolic (LVAWTs), left ventricular posterior wall thickness, systolic  
460 (LVPWTs) and left ventricular posterior wall thickness, diastolic (LVPWTd) were increased  
461 in prediabetic group as assessed with echocardiography, however, other cardiac dimensional  
462 parameters were unchanged (Table 2). The slope of end-diastolic pressure-volume  
463 relationship (EDPVR), which is a very early and sensitive marker of diastolic dysfunction,  
464 was significantly elevated in prediabetes, although other hemodynamic parameters, including

465 blood pressure, were unchanged evidencing the lack of systolic dysfunction or hypertension  
466 (Table 3, Fig. 4B). To uncover the molecular background of the observed mild diastolic  
467 dysfunction, we performed measurements on the common mechanistic contributors of heart  
468 failure (38). On hematoxylin-eosin-stained LV sections increased cardiomyocyte diameter  
469 was detected in prediabetes (Fig. 4 C-D). To characterize components affecting diastolic  
470 function, we analyzed MHC expression. Interestingly, the gene expression of  $\beta$ -MHC was  
471 decreased, and  $\alpha$ -MHC also showed a tendency of decrease ( $p=0.17$ ), the ratio of which  
472 resulted in a strong tendency to decrease in prediabetes. No increase in ANP or BNP gene  
473 expressions (Fig 4. G-H) or in angiotensin-II level (data not shown) was detected in  
474 prediabetes. To evaluate the extent of fibrosis, MA-stained LV sections were analyzed, which  
475 revealed no difference between groups (Fig. 4E). Similarly, we found that gene expression of  
476 type I (COL1) and III (COL3) collagen isoforms were unchanged in the left ventricle (Fig.  
477 4F). These results indicate that mild diastolic dysfunction developed in prediabetic animals  
478 which was associated with a mild hypertrophy (increased LV mass and anterior and posterior  
479 LV wall thickness, increased cardiomyocyte diameter) without signs of fibrosis.

#### 480 **Elevated reactive oxygen species formation in cardiac subsarcolemmal mitochondria in** 481 **prediabetic rats**

482 To investigate whether cardiac mitochondrial disturbances contribute to the observed diastolic  
483 dysfunction, mitochondrial morphology and enzyme activity were analyzed from left  
484 ventricles of prediabetic rats. Our electron microscopy results showed that there is no major  
485 difference in the number of IFM between the groups (Fig. 5, A-B). However, area (CON:  
486  $0.43\pm 0.01$  vs. PRED:  $0.39\pm 0.01 \mu\text{m}^2$ ;  $p<0.05$ ), perimeter (CON:  $2.69\pm 0.02$  vs. PRED:  
487  $2.63\pm 0.03 \mu\text{m}$ ;  $p<0.05$ ) and sphericity (CON:  $0.35\pm 0.01$  vs. PRED:  $0.31\pm 0.01$ ;  $p<0.05$ ) of  
488 IFM are decreased in PRED group. Previous studies indicated that IFM and SSM are affected  
489 by diabetes differentially (35, 80). Therefore, we analyzed our EM imagery containing SSM

490 and found no difference in SSM size, perimeter, or sphericity (data not shown), although, the  
491 statistical power of these analyses was not high enough (n=2 for CON and n=4 for PRED).  
492 Furthermore, we have not seen any major difference in mitochondrial oxygen consumption,  
493 enzyme activities (Table 4-5), Ca-uptake, or membrane potential (data not shown). However,  
494 we have found that hydrogen-peroxide production was increased in the cardiac SSM fraction  
495 with glutamate-malate as a substrate (Fig. 5C), although, there was no difference when  
496 succinate was used as substrate. Interestingly, there was no increase in reactive oxygen  
497 species (ROS) production of the IFM isolated from LV supported either with glutamate-  
498 malate or with succinate (Fig. 5, D-F). As leukocytes are one of the main sources of ROS,  
499 inflammatory mediators were measured. We could find no significant difference in TNF- $\alpha$   
500 (CON:  $1\pm 0.27$  vs. PRED:  $0.59\pm 0.07$ ; ratio normalized to GAPDH;  $p>0.05$ ) and IL-6 (CON:  
501  $1\pm 0.27$  vs. PRED:  $0.69\pm 0.14$ ; ratio normalized to GAPDH;  $p>0.05$ ) mRNA expressions  
502 between groups, which evidence that in our model prediabetes does not elicit cardiac or  
503 systemic inflammation. Furthermore, we have not seen any difference in other markers of  
504 oxidative stress: the expression of p66Shc and tropomyosin oxidation between groups (Fig. 6  
505 B-E). It is known that reactive nitrogen species have important role in deteriorated contractile-  
506 and endothelial function in diabetes (16, 58), therefore, we analyzed whether nitrate stress is  
507 influenced in prediabetes. Nitrotyrosine immunohistology indicated that protein nitrosylation  
508 is increased in prediabetes (Fig. 6A). As CaMKII $\delta$  has been proposed to be activated in  
509 oxidative stress-associated conditions (46), we measured the levels of the active forms of the  
510 kinase which might affect the contractility and relaxation capacity of the heart (49). The  
511 phosphorylation of CaMKII $\delta$  and of its target PLB on Thr<sup>17</sup> was not changed by prediabetes  
512 (Fig. 6, F-H). Similarly, there was no change in the protein expression of SERCA2A in our  
513 model of prediabetes as compared to control animals (Fig. 6J). On the other hand, the level of  
514 p-Ser<sup>16</sup>-PLB showed a tendency for downregulation in prediabetes ( $p=0.08$ ; Fig. 6I).

## 515 **Alterations in cardiac mitofusin-2 expression and mitophagy in prediabetes**

516 To investigate the effect of cardiac mitochondrial dynamics, auto- and mitophagy in  
517 prediabetes, we analyzed protein expression changes. Cardiac expression of the  
518 mitophagy-related protein, BNIP3 was decreased in the prediabetic group in left ventricle  
519 lysates, however, other auto- and mitophagy-related proteins such as Beclin-1, LC3-II,  
520 SQSTM1/p62 and Parkin were unchanged (Fig. 7A; Table 6). Upstream modulators of  
521 autophagy such as Akt, AMPK $\alpha$ , GSK3 $\beta$  and ribosomal S6 protein (a surrogate marker of  
522 mTOR complex activity) were also measured, however, expression or phosphorylation of  
523 these proteins were not different between groups (Fig. 7A; Table 6). Furthermore, the  
524 expression of a mitochondrial fusion-related protein, MFN2 was elevated, however,  
525 expression of DRP1/DLP1 and OPA1 proteins were unchanged in whole left ventricle lysates  
526 in the prediabetic group (Fig. 7B; Table 6). Nonetheless, we measured the expression of  
527 mitochondrial dynamics- and mitophagy-related proteins from SSM and IFM isolated from  
528 left ventricles. No difference was found in the expression of OPA1, LC3-II, SQSTM1/p62 in  
529 isolated cardiac SSM and IFM between groups (Fig. 7, C-D; Table 6). Our results indicate  
530 that mitochondrial dynamics and autophagy/mitophagy were not modulated substantially by  
531 prediabetes, however, the upregulation of MFN2 (increased mitochondrial fusion, tethering to  
532 endoplasmic reticulum) and the downregulation of BNIP3 (decreased mitophagy) may  
533 implicate early changes in mitochondrial homeostasis, which might lead to the accumulation  
534 of dysfunctional mitochondria.

## 535 **Expression of cardiac Bcl-2 decreases in prediabetes**

536 Our study also aimed to explore the effect of prediabetes on apoptosis in the heart.  
537 Prediabetes did not affect the expression of pro-apoptotic caspase-3 and Bax in left ventricles.

538 On the other hand, the anti-apoptotic Bcl-2 was downregulated in prediabetic animals.

539 However, the Bcl-2/Bax ratio was unchanged (Fig. 7F; Table 6).

540 **No changes in cardiac HSPs in prediabetes**

541 We also characterized the effect of prediabetes on the expression and/or phosphorylation of

542 heat shock proteins in the left ventricle. Our results showed no differences in the expression

543 of HSP-60, HSP-70 and HSP-90 or in either phosphorylation or expression of HSP-27 (Fig.

544 7E; Table 6).

545

546

#### 547 **4. Discussion**

548 This is the first comprehensive analysis of the cardiac effects of prediabetes in a non-genetic  
549 rodent model, where we assessed cardiac functions, parameters of hypertrophy, fibrosis,  
550 oxidative and nitrative stress, inflammation, mitochondrial dynamics, autophagy, mitophagy,  
551 markers of myocardial calcium handling, apoptosis, expression of HSPs. In this model of  
552 prediabetes, we evidenced an impaired glucose and insulin tolerance, increased adiposity and  
553 myocardial lipid accumulation, a mild diastolic dysfunction and sensory neuropathy despite  
554 normal fasting plasma glucose and lipid levels. We also observed elevated ROS production in  
555 the SSM, nitrative stress, elevated expression of MFN2, decreased expression of  $\beta$ -MHC, and  
556 phosphorylation of PLB. Furthermore, here we found early signs of dysregulated mitophagy  
557 and decreased mitochondrial size in prediabetes, however, other major markers of  
558 mitochondrial dynamics, auto- and mitophagy, inflammation, or myocardial expression of  
559 apoptotic proteins or HSPs were not modulated by prediabetes.

560 In this study, we used high-fat chow-fed Long-Evans rats treated with a single, low dose STZ.  
561 This setting allowed us to investigate cardiac consequences of a moderate metabolic  
562 derangement, prediabetes, rather than of a severely disturbed glucose and lipid homeostasis,  
563 such as seen in genetically modified models of diabetes, e.g. in *db/db* or *ob/ob* mice (36, 65).  
564 Since it has been reported that LV hypertrophy had a higher prevalence in patients with  
565 diabetes, and that 40-75% of patients with type 1 or type 2 diabetes mellitus presented with  
566 diastolic dysfunction (12, 71), we aimed to investigate whether cardiac function is affected by  
567 prediabetes. Previously it has been shown that diastolic dysfunction was developed in several  
568 pathological condition, however, the underlying mechanisms are still not clearly understood  
569 (38). Here we demonstrated that the deterioration of diastolic function and sensory neuropathy  
570 occurs well before overt diabetes develops, which is accompanied by early signs of cardiac

571 hypertrophy. These findings are in agreement with previous reports showing that neuropathy  
572 might precede the development of a full-fledged diabetes (48), and that high-fat diet-induced  
573 prediabetes increased heart weights and decreased contractile function, as assessed by a  
574 diminished aortic output (23, 29). However, in contrast to our report, plasma triglycerides and  
575 insulin levels were elevated in these studies, highlighting that substantial difference can be  
576 observed between different diet-induced models and stages of prediabetes (29). Furthermore,  
577 it has been described that obesity promoted the hypertrophy-inducing effect of diabetes  
578 regardless of hypertension (26), which could be attributed to adipokines, such as leptin and  
579 resistin (5, 39). Similarly, here we evidenced that even mild obesity (only 18% increase in  
580 body weight was observed in the present study) with an elevated leptin level is sufficient to  
581 induce hypertrophy even without impairment of fasting plasma glucose and lipid levels or  
582 hypertension, which is in agreement with previous reports (23, 29). However, clinical data  
583 seem to contradict these findings, since no increase in the prevalence of LV hypertrophy was  
584 observed in overweight prediabetic patients with impaired fasting glucose and impaired  
585 glucose tolerance (64). Mechanistic studies on how obesity abrogates cardiac function are  
586 scarce. Increased myocardial triglyceride content is associated with diastolic dysfunction in  
587 *ob/ob* mice (18), which is well in line with our findings that the number of lipid particles  
588 increased in the myocardium in prediabetes. Although microRNA-451 has been demonstrated  
589 to promote cardiac hypertrophy and diminished contractile reserves in mice on high-fat diet  
590 (44), further studies are warranted to describe the relationship between cardiac dysfunction  
591 and the disturbed cardiac lipid metabolism in prediabetes. Interestingly, unlike in genetic  
592 models of prediabetes (20), diet-induced prediabetes did not result in an elevation in classical  
593 molecular markers of hypertrophy or conventional signs of fibrosis in the heart as expected in  
594 case of hypertrophy. Moreover, this is the first evidence on decreased  $\beta$ -MHC in prediabetes.  
595 Although the vast majority of publications evidence an increase in  $\beta$ -MHC in diabetes (4, 81),

596 a small number of studies indicate a downregulation of MHC expression in animals with  
597 diverse cardiac or metabolic challenges. For instance, in cardiomyocytes from STZ-treated  
598 rats, total MHC expression was significantly decreased (25). These results indicate that  
599 although in most cardiometabolic derangements expression of the slow MHC isoform  
600 increases, in certain conditions, such as in prediabetes, a general suppression of MHC  
601 expression might be present. The reduction in MHC expression might also contribute to the  
602 observed cardiac dysfunction in prediabetes, however, to uncover its significance and  
603 mechanism, further experiments are warranted.

604 Oxidative stress has a major role in the development of diabetic cardiomyopathy (10, 31),  
605 however, it has not been well described whether it is responsible for the decreased cardiac  
606 function in prediabetes. Here we found an elevated hydrogen peroxide production in SSM,  
607 increased nitrotyrosine formation and an elevated cardiac expression of MFN2. These  
608 findings are in agreement with previous reports, where elevated oxidative stress, such as seen  
609 in our model of prediabetes, leads to an increase in MFN2 in rat vascular smooth muscle cells  
610 (33), and its robust overexpression induced apoptotic cell death in neonatal rat  
611 cardiomyocytes (70). Similarly, in another study, high-fat diet induced oxidative stress and  
612 MFN2 overexpression in the liver of C57BL/6 mice after 16 weeks (27). However, in a  
613 previous study on diet-induced prediabetes, no sign of cardiac mitochondrial oxidative stress  
614 was evidenced in male Wistar rats after 16 weeks (29), which may implicate that  
615 mitochondrial oxidative stress might not be present in all models and stages of prediabetes  
616 and that it might not be the primary driving force of prediabetes-induced cardiac functional  
617 alterations.

618 It is well-established that mitochondria, especially the mitochondrial electron transport chain  
619 is one of the main source of ROS, however, several other intracellular components can  
620 produce ROS in mitochondria (17). For instance, it is known that p66Shc translocation to

621 mitochondria can increase the formation of ROS (22), and NADPH oxidase 4 (NOX4) and  
622 monoamine oxidase (MAO) also have important role in mitochondrial ROS production (8,  
623 43). Although here we observed a moderately increased ROS production in SSM, no  
624 difference can be seen in mitochondrial oxygen consumption between normal and prediabetic  
625 mitochondria (see Table 5), evidencing no impairment in mitochondrial redox chains. It is  
626 currently unknown what mechanism leads to the increased ROS production exclusively in  
627 SSM in prediabetes. In mice on high-fat diet, cardiac mitochondrial ROS production was  
628 elevated, and similarly to our results, mitochondrial oxygen consumption did not change  
629 substantially, while a significant amount of cardiac lipid accumulation was observed (2),  
630 however, the source of ROS has not been identified in this study either. Thus, to reveal the  
631 direct connection between elevated ROS production, mitochondrial-, and cardiac dysfunction,  
632 further studies are warranted.

633 Molecular mechanisms that contribute to hypertrophy and cardiac dysfunction in prediabetes  
634 has not been investigated in detail. In our previous studies on diet-induced  
635 hypercholesterolemia or metabolic syndrome in ZDF rats, we have shown by DNA- and  
636 miRNA microarrays that a multitude of cardiac cellular processes is modulated by these  
637 conditions (67, 77). Similarly, in this study we evidenced changes in several cellular  
638 processes, suggesting that hypertrophy and deteriorated diastolic function in prediabetes  
639 maybe consequences of numerous concurrent alterations in the cardiac homeostasis (see  
640 Figure 8). Characterizing active components of the contractile apparatus and  $Ca^{2+}$   
641 homeostasis, here we observed a tendency to decrease in the Ser<sup>16</sup> phosphorylation of PLB in  
642 prediabetes. In previous studies, decreased phosphorylation of PLB on Ser<sup>16</sup> was  
643 demonstrated to be associated with abnormalities in contraction and relaxation in the diabetic  
644 heart (56, 83). This notion is further supported by the findings of Abdurrachim *et al*, who  
645 demonstrated that phosphorylation of PLB was reduced in the heart of mice with diastolic

646 dysfunction induced by a high-fat diet (2). Therefore, decreased phosphorylation of PLB may  
647 also contribute to the development of early diastolic dysfunction we uncovered in prediabetes.  
648 Increased activity and expression of CaMKII $\delta$  and reduced phosphorylation of PLB by  
649 CaMKII $\delta$  have been found to be associated with contractile dysfunction, diabetes (47, 49),  
650 and fructose-rich diet-induced prediabetes (73). In our model, expression and phosphorylation  
651 of CaMKII $\delta$ , and phosphorylation of PLB on Thr<sup>17</sup> were unchanged. This is in contrast with  
652 previous findings which have reported the phosphorylation of CaMKII $\delta$  being increased in the  
653 heart of STZ-treated diabetic rats (69, 74), although, in these reports, a significant  
654 hyperglycemia was present, which was shown to facilitate the activation of CaMKII $\delta$  (28).  
655 Apoptosis is considered to be one of the hallmarks of diabetic cardiomyopathy and it is  
656 induced by oxidative stress in diabetes (10, 76). It has been described that experimental  
657 diabetes induces upregulation of pro-apoptotic, and downregulation of anti-apoptotic proteins  
658 (3, 82), however, no data has been available on the cardiac apoptosis in prediabetes. In the  
659 present study, we show a modest downregulation of Bcl-2, however, no change in Bcl-2/Bax  
660 ratio, and in caspase-3 expression was detected in prediabetic animals. Thus, our data suggest  
661 an early dysregulation of pro- and antiapoptotic proteins in prediabetes, however, they do not  
662 evidence a gross induction of apoptosis in prediabetes. Tropomyosin is prone to loss of  
663 function by oxidative modifications that are associated with the severity of heart failure in  
664 humans (14, 15). In this study, oxidized tropomyosin content of the heart was not modulated  
665 by prediabetes. These data suggest that neither the CaMKII $\delta$  pathway, apoptosis induction,  
666 nor tropomyosin oxidation are responsible for the diastolic dysfunction observed in  
667 prediabetes.

668 Here we also demonstrate an early dysregulation of mitochondrial fusion and mitophagy first  
669 in the literature, as evidenced by an elevated MFN2 and an attenuated BNIP3 expression in  
670 prediabetes, however, other canonical markers of autophagy, mitophagy and apoptosis were

671 unaffected. Similarly, right atrial myocardial samples of type-2 diabetic patients presenting no  
672 signs of overt cardiomyopathy the expression of the majority of mitochondrial dynamics- and  
673 autophagy-related proteins was not elevated, except for that of ATG5 and MFN1 (53).  
674 Therefore, we can assume that only major disturbances in glucose and lipid homeostasis, such  
675 as seen in untreated patients or in genetic models of diabetes, might be a powerful enough  
676 signal to extensively modulate cardiac autophagy, mitophagy, or mitochondrial dynamics,  
677 which might result in grossly deteriorated cardiac function. Moreover, experimental systemic  
678 sensory neuropathy by itself has been previously shown to cause diastolic dysfunction and  
679 global gene expression changes in the rat heart (7, 84). Therefore, prediabetes-induced  
680 sensory neuropathy observed in the present study might also contribute to the diabetic  
681 cardiomyopathy.

682 Furthermore, this is the first report to show that prediabetes does not modulate cardiac  
683 expression of HSP-60, HSP-70 and HSP-90 and phosphorylation or expression of HSP-27. In  
684 contrast, in STZ-induced diabetes, increased levels of HSP-70 has been detected in the rat  
685 heart (75), and increased level of circulating HSP-60 found in diabetic patients (68),  
686 suggesting that in advanced stages of diabetes HSPs might be involved in the development of  
687 cardiac dysfunction. However, our data suggests no role of HSPs in prediabetes in the heart.

## 688 **Conclusions**

689 Taken together, this study emphasizes that parallel occurrence of several abnormalities of  
690 metabolic, oxidative and contractile functions might trigger cardiac pathological changes  
691 characteristic to prediabetes well before hyperglycemia or major metabolic derangements  
692 occur, and that preventing these abnormalities might be of importance for future therapies of  
693 cardiac pathologies observed in early metabolic diseases such as prediabetes.

694

695

## 696 **5. Acknowledgements:**

697 We would like to thank to Melinda Károlyi-Szabó, Jenőné Benkes, Henriett Biró, Ildikó  
698 Horváth, Teréz Bagoly, Sebestyén Tuza and Anikó Perkecz for technical assistance.

## 699 **Grants**

700 This work was supported by the European Foundation for the Study of Diabetes (EFSD) New  
701 Horizons Collaborative Research Initiative from European Association for the Study of  
702 Diabetes (EASD) and Hungarian Scientific Research Fund (OTKA K 109737, PD100245 to  
703 TR), and Slovak Scientific Grant Agency (VEGA1/0638/12). ZG, TR and KSZ holds a “János  
704 Bolyai Research Scholarship” from the Hungarian Academy of Sciences and ZVV was  
705 supported by the Rosztoczy Foundation. PF is a Szentágothai Fellow of the National Program  
706 of Excellence (TAMOP 4.2.4. A/2-11-1-2012-0001). TB is supported by the European  
707 Cooperation in Science and Technology (COST-BM1203-STSM 090515-058721). KB and  
708 RS are supported by the German Research Foundation (BO-2955/2-1 and SCHU 843/9-1).

## 709 **Disclosures**

710 All authors read and approved the final manuscript. The authors have reported that they have  
711 no relationships relevant to the contents of this paper to disclose.

## 712 **Author contributions**

713 GK, ZVV, TB, MB, TR, TK, MA performed experiments, assisted with analyses of results  
714 and interpretation and writing. KB, RT, AO and LD assisted with analyses of results,  
715 interpretation and writing the manuscript. AA, BM, ZSH, DM, SZK, PH, SR, LT and PP  
716 contributed to experiments, analysis, and interpretation of data. GK, ZVV, TB, RT, AO,

717 CSM, LA, and ST performed experiments with animals. PF, RS, ZVV and ZG designed the  
718 experiments, drafted and edited the manuscript.

719

721 **6- References:**

- 722 1. Diagnosis and classification of diabetes mellitus. *Diabetes care* 37 Suppl 1: S81-90,  
723 2014.
- 724 2. **Abdurrachim D, Ciapaite J, Wessels B, Nabben M, Luiken JJ, Nicolay K, and**  
725 **Prompers JJ.** Cardiac diastolic dysfunction in high-fat diet fed mice is associated with  
726 lipotoxicity without impairment of cardiac energetics in vivo. *Biochimica et biophysica acta*  
727 1842: 1525-1537, 2014.
- 728 3. **Amin AH, El-Missiry MA, and Othman AI.** Melatonin ameliorates metabolic risk  
729 factors, modulates apoptotic proteins, and protects the rat heart against diabetes-induced  
730 apoptosis. *Eur J Pharmacol* 747: 166-173, 2015.
- 731 4. **Aragno M, Mastrocola R, Medana C, Catalano MG, Vercellinato I, Danni O,**  
732 **and Boccuzzi G.** Oxidative stress-dependent impairment of cardiac-specific transcription  
733 factors in experimental diabetes. *Endocrinology* 147: 5967-5974, 2006.
- 734 5. **Barouch LA, Berkowitz DE, Harrison RW, O'Donnell CP, and Hare JM.**  
735 Disruption of leptin signaling contributes to cardiac hypertrophy independently of body  
736 weight in mice. *Circulation* 108: 754-759, 2003.
- 737 6. **Barr EL, Zimmet PZ, Welborn TA, Jolley D, Magliano DJ, Dunstan DW,**  
738 **Cameron AJ, Dwyer T, Taylor HR, Tonkin AM, Wong TY, McNeil J, and Shaw JE.**  
739 Risk of cardiovascular and all-cause mortality in individuals with diabetes mellitus, impaired  
740 fasting glucose, and impaired glucose tolerance: the Australian Diabetes, Obesity, and  
741 Lifestyle Study (AusDiab). *Circulation* 116: 151-157, 2007.
- 742 7. **Bencsik P, Kupai K, Giricz Z, Gorbe A, Huliak I, Furst S, Dux L, Csont T,**  
743 **Jancso G, and Ferdinandy P.** Cardiac capsaicin-sensitive sensory nerves regulate  
744 myocardial relaxation via S-nitrosylation of SERCA: role of peroxynitrite. *Br J Pharmacol*  
745 153: 488-496, 2008.
- 746 8. **Bianchi P, Kunduzova O, Masini E, Cambon C, Bani D, Raimondi L, Seguelas**  
747 **MH, Nistri S, Colucci W, Leducq N, and Parini A.** Oxidative stress by monoamine oxidase  
748 mediates receptor-independent cardiomyocyte apoptosis by serotonin and postischemic  
749 myocardial injury. *Circulation* 112: 3297-3305, 2005.
- 750 9. **Bjorndal B, Burri L, Staalesen V, Skorve J, and Berge RK.** Different adipose  
751 depots: their role in the development of metabolic syndrome and mitochondrial response to  
752 hypolipidemic agents. *Journal of obesity* 2011: 490650, 2011.
- 753 10. **Boudina S, and Abel ED.** Diabetic cardiomyopathy, causes and effects. *Reviews in*  
754 *endocrine & metabolic disorders* 11: 31-39, 2010.
- 755 11. **Bradford MM.** A rapid and sensitive method for the quantitation of microgram  
756 quantities of protein utilizing the principle of protein-dye binding. *Analytical biochemistry* 72:  
757 248-254, 1976.
- 758 12. **Brooks BA, Franjic B, Ban CR, Swaraj K, Yue DK, Celermajer DS, and Twigg**  
759 **SM.** Diastolic dysfunction and abnormalities of the microcirculation in type 2 diabetes.  
760 *Diabetes, obesity & metabolism* 10: 739-746, 2008.
- 761 13. **Cai L, and Kang YJ.** Cell death and diabetic cardiomyopathy. *Cardiovascular*  
762 *toxicology* 3: 219-228, 2003.
- 763 14. **Canton M, Menazza S, Sheeran FL, Polverino de Laureto P, Di Lisa F, and Pepe**  
764 **S.** Oxidation of myofibrillar proteins in human heart failure. *Journal of the American College*  
765 *of Cardiology* 57: 300-309, 2011.

- 766 15. **Canton M, Neverova I, Menabo R, Van Eyk J, and Di Lisa F.** Evidence of  
767 myofibrillar protein oxidation induced by postischemic reperfusion in isolated rat hearts.  
768 *American journal of physiology Heart and circulatory physiology* 286: H870-877, 2004.
- 769 16. **Cassuto J, Dou H, Czikora I, Szabo A, Patel VS, Kamath V, Belin de Chantemele  
770 E, Feher A, Romero MJ, and Bagi Z.** Peroxynitrite disrupts endothelial caveolae leading to  
771 eNOS uncoupling and diminished flow-mediated dilation in coronary arterioles of diabetic  
772 patients. *Diabetes* 63: 1381-1393, 2014.
- 773 17. **Chen YR, and Zweier JL.** Cardiac mitochondria and reactive oxygen species  
774 generation. *Circ Res* 114: 524-537, 2014.
- 775 18. **Christoffersen C, Bollano E, Lindegaard ML, Bartels ED, Goetze JP, Andersen  
776 CB, and Nielsen LB.** Cardiac lipid accumulation associated with diastolic dysfunction in  
777 obese mice. *Endocrinology* 144: 3483-3490, 2003.
- 778 19. **Csont T, Bereczki E, Bencsik P, Fodor G, Gorbe A, Zvara A, Csonka C, Puskas  
779 LG, Santha M, and Ferdinandy P.** Hypercholesterolemia increases myocardial oxidative  
780 and nitrosative stress thereby leading to cardiac dysfunction in apoB-100 transgenic mice.  
781 *Cardiovasc Res* 76: 100-109, 2007.
- 782 20. **D'Souza A, Howarth FC, Yanni J, Dobryznski H, Boyett MR, Adeghate E,  
783 Bidasee KR, and Singh J.** Left ventricle structural remodelling in the prediabetic Goto-  
784 Kakizaki rat. *Experimental physiology* 96: 875-888, 2011.
- 785 21. **DeFronzo RA, and Abdul-Ghani M.** Assessment and treatment of cardiovascular  
786 risk in prediabetes: impaired glucose tolerance and impaired fasting glucose. *The American  
787 journal of cardiology* 108: 3b-24b, 2011.
- 788 22. **Di Lisa F, Giorgio M, Ferdinandy P, and Schulz R.** New aspects of p66Shc in  
789 ischemia reperfusion injury and cardiovascular diseases. *Br J Pharmacol* 2016.
- 790 23. **du Toit EF, Smith W, Muller C, Strijdom H, Stouthammer B, Woodiwiss AJ,  
791 Norton GR, and Lochner A.** Myocardial susceptibility to ischemic-reperfusion injury in a  
792 prediabetic model of dietary-induced obesity. *American journal of physiology Heart and  
793 circulatory physiology* 294: H2336-2343, 2008.
- 794 24. **Duncan JG.** Mitochondrial dysfunction in diabetic cardiomyopathy. *Biochimica et  
795 biophysica acta* 1813: 1351-1359, 2011.
- 796 25. **Dyntar D, Sergeev P, Klisic J, Ambuhl P, Schaub MC, and Donath MY.** High  
797 glucose alters cardiomyocyte contacts and inhibits myofibrillar formation. *The Journal of  
798 clinical endocrinology and metabolism* 91: 1961-1967, 2006.
- 799 26. **Eguchi K, Boden-Albala B, Jin Z, Rundek T, Sacco RL, Homma S, and Di Tullio  
800 MR.** Association between diabetes mellitus and left ventricular hypertrophy in a multiethnic  
801 population. *The American journal of cardiology* 101: 1787-1791, 2008.
- 802 27. **Enos RT, Velazquez KT, and Murphy EA.** Insight into the impact of dietary  
803 saturated fat on tissue-specific cellular processes underlying obesity-related diseases. *The  
804 Journal of nutritional biochemistry* 25: 600-612, 2014.
- 805 28. **Erickson JR, Pereira L, Wang L, Han G, Ferguson A, Dao K, Copeland RJ,  
806 Despa F, Hart GW, Ripplinger CM, and Bers DM.** Diabetic hyperglycaemia activates  
807 CaMKII and arrhythmias by O-linked glycosylation. *Nature* 502: 372-376, 2013.
- 808 29. **Essop MF, Anna Chan WY, Valle A, Garcia-Palmer FJ, and Du Toit EF.**  
809 Impaired contractile function and mitochondrial respiratory capacity in response to oxygen  
810 deprivation in a rat model of pre-diabetes. *Acta physiologica (Oxford, England)* 197: 289-296,  
811 2009.
- 812 30. **Fonseca VA.** Identification and treatment of prediabetes to prevent progression to type  
813 2 diabetes. *Clinical cornerstone* 9: 51-59; discussion 60-51, 2008.
- 814 31. **Frustaci A, Kajstura J, Chimenti C, Jakoniuk I, Leri A, Maseri A, Nadal-Ginard  
815 B, and Anversa P.** Myocardial cell death in human diabetes. *Circ Res* 87: 1123-1132, 2000.

- 816 32. **Galloway CA, and Yoon Y.** Mitochondrial dynamics in diabetic cardiomyopathy.  
817 *Antioxid Redox Signal* 22: 1545-1562, 2015.
- 818 33. **Guo X, Chen KH, Guo Y, Liao H, Tang J, and Xiao RP.** Mitofusin 2 triggers  
819 vascular smooth muscle cell apoptosis via mitochondrial death pathway. *Circ Res* 101: 1113-  
820 1122, 2007.
- 821 34. **Harms M, and Seale P.** Brown and beige fat: development, function and therapeutic  
822 potential. *Nature medicine* 19: 1252-1263, 2013.
- 823 35. **Holloway GP, Snook LA, Harris RJ, Glatz JF, Luiken JJ, and Bonen A.** In obese  
824 Zucker rats, lipids accumulate in the heart despite normal mitochondrial content, morphology  
825 and long-chain fatty acid oxidation. *J Physiol* 589: 169-180, 2011.
- 826 36. **Hsueh W, Abel ED, Breslow JL, Maeda N, Davis RC, Fisher EA, Dansky H,  
827 McClain DA, McIndoe R, Wassef MK, Rabadan-Diehl C, and Goldberg IJ.** Recipes for  
828 creating animal models of diabetic cardiovascular disease. *Circ Res* 100: 1415-1427, 2007.
- 829 37. **Kass D.** Clinical ventricular pathophysiology: a pressure-volume view. *Warltier DC  
830 Baltimore, MD: Williams & Wilkins* 131-151, 1995.
- 831 38. **Kass DA, Bronzwaer JG, and Paulus WJ.** What mechanisms underlie diastolic  
832 dysfunction in heart failure? *Circ Res* 94: 1533-1542, 2004.
- 833 39. **Kim M, Oh JK, Sakata S, Liang I, Park W, Hajjar RJ, and Lebeche D.** Role of  
834 resistin in cardiac contractility and hypertrophy. *J Mol Cell Cardiol* 45: 270-280, 2008.
- 835 40. **Kleiner DE, Brunt EM, Van Natta M, Behling C, Contos MJ, Cummings OW,  
836 Ferrell LD, Liu YC, Torbenson MS, Unalp-Arida A, Yeh M, McCullough AJ, and  
837 Sanyal AJ.** Design and validation of a histological scoring system for nonalcoholic fatty liver  
838 disease. *Hepatology (Baltimore, Md)* 41: 1313-1321, 2005.
- 839 41. **Kobayashi S, and Liang Q.** Autophagy and mitophagy in diabetic cardiomyopathy.  
840 *Biochimica et biophysica acta* 1852: 252-261, 2015.
- 841 42. **Kovacs A, Olah A, Lux A, Matyas C, Nemeth BT, Kellermayer D, Ruppert M,  
842 Torok M, Szabo L, Meltzer A, Assabiny A, Birtalan E, Merkely B, and Radovits T.**  
843 Strain and strain rate by speckle-tracking echocardiography correlate with pressure-volume  
844 loop-derived contractility indices in a rat model of athlete's heart. *American journal of  
845 physiology Heart and circulatory physiology* 308: H743-748, 2015.
- 846 43. **Kuroda J, Ago T, Matsushima S, Zhai P, Schneider MD, and Sadoshima J.**  
847 NADPH oxidase 4 (Nox4) is a major source of oxidative stress in the failing heart. *Proc Natl  
848 Acad Sci U S A* 107: 15565-15570, 2010.
- 849 44. **Kuwabara Y, Horie T, Baba O, Watanabe S, Nishiga M, Usami S, Izuhara M,  
850 Nakao T, Nishino T, Otsu K, Kita T, Kimura T, and Ono K.** MicroRNA-451 exacerbates  
851 lipotoxicity in cardiac myocytes and high-fat diet-induced cardiac hypertrophy in mice  
852 through suppression of the LKB1/AMPK pathway. *Circ Res* 116: 279-288, 2015.
- 853 45. **Lewis CE, McTigue KM, Burke LE, Poirier P, Eckel RH, Howard BV, Allison  
854 DB, Kumanyika S, and Pi-Sunyer FX.** Mortality, health outcomes, and body mass index in  
855 the overweight range: a science advisory from the American Heart Association. *Circulation*  
856 119: 3263-3271, 2009.
- 857 46. **Luczak ED, and Anderson ME.** CaMKII oxidative activation and the pathogenesis  
858 of cardiac disease. *J Mol Cell Cardiol* 73: 112-116, 2014.
- 859 47. **Luo M, Guan X, Luczak ED, Lang D, Kutschke W, Gao Z, Yang J, Glynn P,  
860 Sossalla S, Swaminathan PD, Weiss RM, Yang B, Rokita AG, Maier LS, Efimov IR,  
861 Hund TJ, and Anderson ME.** Diabetes increases mortality after myocardial infarction by  
862 oxidizing CaMKII. *J Clin Invest* 123: 1262-1274, 2013.
- 863 48. **Lupachyk S, Watcho P, Obrosova AA, Stavniichuk R, and Obrosova IG.**  
864 Endoplasmic reticulum stress contributes to prediabetic peripheral neuropathy. *Experimental  
865 neurology* 247: 342-348, 2013.

- 866 49. **Maier LS, and Bers DM.** Role of Ca<sup>2+</sup>/calmodulin-dependent protein kinase  
867 (CaMK) in excitation-contraction coupling in the heart. *Cardiovasc Res* 73: 631-640, 2007.
- 868 50. **Mansor LS, Gonzalez ER, Cole MA, Tyler DJ, Beeson JH, Clarke K, Carr CA,**  
869 **and Heather LC.** Cardiac metabolism in a new rat model of type 2 diabetes using high-fat  
870 diet with low dose streptozotocin. *Cardiovascular diabetology* 12: 136, 2013.
- 871 51. **Mizushige K, Yao L, Noma T, Kiyomoto H, Yu Y, Hosomi N, Ohmori K, and**  
872 **Matsuo H.** Alteration in left ventricular diastolic filling and accumulation of myocardial  
873 collagen at insulin-resistant prediabetic stage of a type II diabetic rat model. *Circulation* 101:  
874 899-907, 2000.
- 875 52. **Mohanty JG, Jaffe JS, Schulman ES, and Raible DG.** A highly sensitive  
876 fluorescent micro-assay of H<sub>2</sub>O<sub>2</sub> release from activated human leukocytes using a  
877 dihydroxyphenoxazine derivative. *Journal of immunological methods* 202: 133-141, 1997.
- 878 53. **Montaigne D, Marechal X, Coisne A, Debry N, Modine T, Fayad G, Potelle C, El**  
879 **Arid JM, Mouton S, Sebti Y, Duez H, Preau S, Remy-Jouet I, Zerimech F, Koussa M,**  
880 **Richard V, Neviere R, Edme JL, Lefebvre P, and Staels B.** Myocardial contractile  
881 dysfunction is associated with impaired mitochondrial function and dynamics in type 2  
882 diabetic but not in obese patients. *Circulation* 130: 554-564, 2014.
- 883 54. **Nathan DM, Davidson MB, DeFronzo RA, Heine RJ, Henry RR, Pratley R, and**  
884 **Zinman B.** Impaired fasting glucose and impaired glucose tolerance: implications for care.  
885 *Diabetes care* 30: 753-759, 2007.
- 886 55. **Orhan CE, Onal A, Uyanikgil Y, and Ulker S.** Antihyperalgesic and antiallodynic  
887 effect of sirolimus in rat model of adjuvant arthritis. *Eur J Pharmacol* 705: 35-41, 2013.
- 888 56. **Ouwens DM, Boer C, Fodor M, de Galan P, Heine RJ, Maassen JA, and Diamant**  
889 **M.** Cardiac dysfunction induced by high-fat diet is associated with altered myocardial insulin  
890 signalling in rats. *Diabetologia* 48: 1229-1237, 2005.
- 891 57. **Pacher P, Nagayama T, Mukhopadhyay P, Batkai S, and Kass DA.** Measurement  
892 of cardiac function using pressure-volume conductance catheter technique in mice and rats.  
893 *Nature protocols* 3: 1422-1434, 2008.
- 894 58. **Pechanova O, Varga ZV, Cebova M, Giricz Z, Pacher P, and Ferdinandy P.**  
895 Cardiac NO signalling in the metabolic syndrome. *Br J Pharmacol* 172: 1415-1433, 2015.
- 896 59. **Pereira L, Ruiz-Hurtado G, Rueda A, Mercadier JJ, Benitah JP, and Gomez AM.**  
897 Calcium signaling in diabetic cardiomyocytes. *Cell calcium* 56: 372-380, 2014.
- 898 60. **Radovits T, Korkmaz S, Loganathan S, Barnucz E, Bomicke T, Arif R, Karck M,**  
899 **and Szabo G.** Comparative investigation of the left ventricular pressure-volume relationship  
900 in rat models of type 1 and type 2 diabetes mellitus. *American journal of physiology Heart*  
901 *and circulatory physiology* 297: H125-133, 2009.
- 902 61. **Radovits T, Korkmaz S, Matyas C, Olah A, Nemeth BT, Pali S, Hirschberg K,**  
903 **Zubarevich A, Gwanmesia PN, Li S, Loganathan S, Barnucz E, Merkely B, and Szabo**  
904 **G.** An altered pattern of myocardial histopathological and molecular changes underlies the  
905 different characteristics of type-1 and type-2 diabetic cardiac dysfunction. *Journal of diabetes*  
906 *research* 2015: 728741, 2015.
- 907 62. **Radovits T, Olah A, Lux A, Nemeth BT, Hidi L, Birtalan E, Kellermayer D,**  
908 **Matyas C, Szabo G, and Merkely B.** Rat model of exercise-induced cardiac hypertrophy:  
909 hemodynamic characterization using left ventricular pressure-volume analysis. *American*  
910 *journal of physiology Heart and circulatory physiology* 305: H124-134, 2013.
- 911 63. **Reffellmann T, and Kloner RA.** Transthoracic echocardiography in rats. Evaluation of  
912 commonly used indices of left ventricular dimensions, contractile performance, and  
913 hypertrophy in a genetic model of hypertrophic heart failure (SHHF-Mcc-facp-Rats) in  
914 comparison with Wistar rats during aging. *Basic Res Cardiol* 98: 275-284, 2003.

- 915 64. **Rerkpattanapipat P, D'Agostino RB, Jr., Link KM, Shahar E, Lima JA, Bluemke**  
916 **DA, Sinha S, Herrington DM, and Hundley WG.** Location of arterial stiffening differs in  
917 those with impaired fasting glucose versus diabetes: implications for left ventricular  
918 hypertrophy from the Multi-Ethnic Study of Atherosclerosis. *Diabetes* 58: 946-953, 2009.
- 919 65. **Russell JC, and Proctor SD.** Small animal models of cardiovascular disease: tools for  
920 the study of the roles of metabolic syndrome, dyslipidemia, and atherosclerosis.  
921 *Cardiovascular pathology : the official journal of the Society for Cardiovascular Pathology*  
922 15: 318-330, 2006.
- 923 66. **Ryden L, Grant PJ, Anker SD, Berne C, Cosentino F, Danchin N, Deaton C,**  
924 **Escaned J, Hammes HP, Huikuri H, Marre M, Marx N, Mellbin L, Ostergren J,**  
925 **Patrono C, Seferovic P, Uva MS, Taskinen MR, Tendera M, Tuomilehto J, Valensi P,**  
926 **Zamorano JL, Zamorano JL, Achenbach S, Baumgartner H, Bax JJ, Bueno H, Dean V,**  
927 **Deaton C, Erol C, Fagard R, Ferrari R, Hasdai D, Hoes AW, Kirchhof P, Knuuti J,**  
928 **Kolh P, Lancellotti P, Linhart A, Nihoyannopoulos P, Piepoli MF, Ponikowski P, Sirnes**  
929 **PA, Tamargo JL, Tendera M, Torbicki A, Wijns W, Windecker S, De Backer G, Sirnes**  
930 **PA, Ezquerra EA, Avogaro A, Badimon L, Baranova E, Baumgartner H, Betteridge J,**  
931 **Ceriello A, Fagard R, Funck-Brentano C, Gulba DC, Hasdai D, Hoes AW, Kjekshus JK,**  
932 **Knuuti J, Kolh P, Lev E, Mueller C, Neyses L, Nilsson PM, Perk J, Ponikowski P,**  
933 **Reiner Z, Sattar N, Schachinger V, Scheen A, Schirmer H, Stromberg A, Sudzhaeva S,**  
934 **Tamargo JL, Viigimaa M, Vlachopoulos C, and Xuereb RG.** ESC Guidelines on diabetes,  
935 pre-diabetes, and cardiovascular diseases developed in collaboration with the EASD: the Task  
936 Force on diabetes, pre-diabetes, and cardiovascular diseases of the European Society of  
937 Cardiology (ESC) and developed in collaboration with the European Association for the  
938 Study of Diabetes (EASD). *European heart journal* 34: 3035-3087, 2013.
- 939 67. **Sarkozy M, Zvara A, Gyemant N, Fekete V, Kocsis GF, Pipis J, Szucs G, Csonka**  
940 **C, Puskas LG, Ferdinandy P, and Csont T.** Metabolic syndrome influences cardiac gene  
941 expression pattern at the transcript level in male ZDF rats. *Cardiovascular diabetology* 12: 16,  
942 2013.
- 943 68. **Shamaei-Tousi A, Stephens JW, Bin R, Cooper JA, Steptoe A, Coates AR,**  
944 **Henderson B, and Humphries SE.** Association between plasma levels of heat shock protein  
945 60 and cardiovascular disease in patients with diabetes mellitus. *European heart journal* 27:  
946 1565-1570, 2006.
- 947 69. **Shao CH, Wehrens XH, Wyatt TA, Parbhu S, Rozanski GJ, Patel KP, and**  
948 **Bidasee KR.** Exercise training during diabetes attenuates cardiac ryanodine receptor  
949 dysregulation. *Journal of applied physiology (Bethesda, Md : 1985)* 106: 1280-1292, 2009.
- 950 70. **Shen T, Zheng M, Cao C, Chen C, Tang J, Zhang W, Cheng H, Chen KH, and**  
951 **Xiao RP.** Mitofusin-2 is a major determinant of oxidative stress-mediated heart muscle cell  
952 apoptosis. *J Biol Chem* 282: 23354-23361, 2007.
- 953 71. **Shivalkar B, Dhondt D, Goovaerts I, Van Gaal L, Bartunek J, Van Crombrugge**  
954 **P, and Vrints C.** Flow mediated dilatation and cardiac function in type 1 diabetes mellitus.  
955 *The American journal of cardiology* 97: 77-82, 2006.
- 956 72. **Soetkamp D, Nguyen TT, Menazza S, Hirschhauser C, Hendgen-Cotta UB,**  
957 **Rassaf T, Schluter KD, Boengler K, Murphy E, and Schulz R.** S-nitrosation of  
958 mitochondrial connexin 43 regulates mitochondrial function. *Basic Res Cardiol* 109: 433,  
959 2014.
- 960 73. **Sommese L, Valverde CA, Blanco P, Castro MC, Rueda OV, Kaetzel M, Dedman**  
961 **J, Anderson ME, Mattiazzi A, and Palomeque J.** Ryanodine receptor phosphorylation by  
962 CaMKII promotes spontaneous Ca(2+) release events in a rodent model of early stage  
963 diabetes: The arrhythmogenic substrate. *International journal of cardiology* 202: 394-406,  
964 2016.

- 965 74. **Tuncay E, Zeydanli EN, and Turan B.** Cardioprotective effect of propranolol on  
966 diabetes-induced altered intracellular Ca<sup>2+</sup> signaling in rat. *Journal of bioenergetics and*  
967 *biomembranes* 43: 747-756, 2011.
- 968 75. **Ugurlucan M, Erer D, Karatepe O, Ziyade S, Haholu A, Gungor Ugurlucan F,**  
969 **Filizcan U, Tireli E, Dayioglu E, and Alpagut U.** Glutamine enhances the heat shock  
970 protein 70 expression as a cardioprotective mechanism in left heart tissues in the presence of  
971 diabetes mellitus. *Expert opinion on therapeutic targets* 14: 1143-1156, 2010.
- 972 76. **Varga ZV, Giricz Z, Liaudet L, Hasko G, Ferdinandy P, and Pacher P.** Interplay  
973 of oxidative, nitrosative/nitrative stress, inflammation, cell death and autophagy in diabetic  
974 cardiomyopathy. *Biochimica et biophysica acta* 1852: 232-242, 2015.
- 975 77. **Varga ZV, Kupai K, Szucs G, Gaspar R, Paloczi J, Farago N, Zvara A, Puskas**  
976 **LG, Razga Z, Tiszlavicz L, Bencsik P, Gorbe A, Csonka C, Ferdinandy P, and Csont T.**  
977 MicroRNA-25-dependent up-regulation of NADPH oxidase 4 (NOX4) mediates  
978 hypercholesterolemia-induced oxidative/nitrative stress and subsequent dysfunction in the  
979 heart. *J Mol Cell Cardiol* 62: 111-121, 2013.
- 980 78. **Verkhatsky A, and Fernyhough P.** Mitochondrial malfunction and Ca<sup>2+</sup>  
981 dyshomeostasis drive neuronal pathology in diabetes. *Cell calcium* 44: 112-122, 2008.
- 982 79. **Wild S, Roglic G, Green A, Sicree R, and King H.** Global prevalence of diabetes:  
983 estimates for the year 2000 and projections for 2030. *Diabetes care* 27: 1047-1053, 2004.
- 984 80. **Williamson CL, Dabkowski ER, Baseler WA, Croston TL, Alway SE, and**  
985 **Hollander JM.** Enhanced apoptotic propensity in diabetic cardiac mitochondria: influence of  
986 subcellular spatial location. *American journal of physiology Heart and circulatory physiology*  
987 298: H633-642, 2010.
- 988 81. **Yagi K, Kim S, Wanibuchi H, Yamashita T, Yamamura Y, and Iwao H.**  
989 Characteristics of diabetes, blood pressure, and cardiac and renal complications in Otsuka  
990 Long-Evans Tokushima Fatty rats. *Hypertension* 29: 728-735, 1997.
- 991 82. **Yu W, Zha W, Guo S, Cheng H, Wu J, and Liu C.** Flos Puerariae extract prevents  
992 myocardial apoptosis via attenuation oxidative stress in streptozotocin-induced diabetic mice.  
993 *PloS one* 9: e98044, 2014.
- 994 83. **Zhong Y, Ahmed S, Grupp IL, and Matlib MA.** Altered SR protein expression  
995 associated with contractile dysfunction in diabetic rat hearts. *American journal of physiology*  
996 *Heart and circulatory physiology* 281: H1137-1147, 2001.
- 997 84. **Zvara A, Bencsik P, Fodor G, Csont T, Hackler L, Jr., Dux M, Furst S, Jancso G,**  
998 **Puskas LG, and Ferdinandy P.** Capsaicin-sensitive sensory neurons regulate myocardial  
999 function and gene expression pattern of rat hearts: a DNA microarray study. *FASEB journal :*  
1000 *official publication of the Federation of American Societies for Experimental Biology* 20:  
1001 160-162, 2006.

## 1002 **2. Figure captions:**

1003 **Fig. 1. Experimental protocol.** Long-Evans rats were fed with either control (CON) diet for  
1004 21 weeks, or with high-fat diet and treated with 20 mg/kg streptozotocin (STZ) at week 4  
1005 (PRED) to induce prediabetes. Body weights were measured weekly and blood samples were  
1006 taken from the saphenic vein every second week. Sensory neuropathy was measured at week  
1007 15. Oral glucose tolerance test (OGTT), insulin tolerance test (ITT) and computer tomography

1008 (CT) were performed at week 20. Echocardiography, hemodynamic analysis and parameters  
1009 of mitochondrial function were measured at week 21 of diet. Tissue sampling was performed  
1010 after terminal procedures.

1011 **Fig. 2. High-fat feeding with a single low dose STZ treatment increase adiposity.** Changes  
1012 in body weight during the experiment (A) and body weight data after 21 weeks (B). Axial  
1013 representative CT slice from the middle of 4<sup>th</sup> lumbal spine. Red color indicates the  
1014 segmented Volume-of-Interests (VOIs) showing the volume of fat in the control (CON) and  
1015 prediabetic (PRED) rats (C). Whole body fat volume to body weight ratio at week 20 (D).  
1016 Representative transmission electron micrographs of myocardial lipid droplets (E; white  
1017 arrows) and number of lipid droplets in CON and PRED cardiomyocytes (F). Magnification  
1018 7,500×; scale bar 1 μm. Epididymal fat tissue (G) and interscapular brown adipose tissue  
1019 (BAT) (I) weight to body weight ratios. Hematoxylin-Eosin (HE) and Masson's trichrome  
1020 (MA) staining of liver sections (H). Magnification 200×; scale bar 100 μm. Data are  
1021 means±SEM N= 3-19 per group (\*p<0.05).

1022 **Fig. 3. Alterations in glucose homeostasis indicate the development of a prediabetes in**  
1023 **streptozotocin-treated and high-fat-fed rats at week 21.** Fasting blood glucose levels  
1024 during the experiment (A) and at week 20 (B). Oral glucose tolerance test (OGTT) (C-D) and  
1025 insulin tolerance test (ITT) (E-F) results at week 20 of the diet. Insulin content of pancreas at  
1026 week 21 (G). Data are means±SEM, n=6-19 per group (\*: p<0.05).

1027 **Fig. 4. Characterization of cardiac function, myocardial morphology and fibrosis in**  
1028 **prediabetic rats.** Quantification of heart weights after 21 weeks (A). Representative pressure-  
1029 volume loops and slope of EDPVR in CON and PRED group (B). HE and MA staining of  
1030 myocardial sections (C) and quantification of cardiomyocyte diameter (D) and level of  
1031 fibrosis (E) in control (CON) and prediabetic (PRED) rats. Magnification 200×; scale bar 100

1032  $\mu\text{m}$ . Quantification of COL1, COL3 (*F*), ANP, BNP (*G*),  $\alpha$ -MHC,  $\beta$ -MHC gene expressions  
1033 and  $\alpha$ - to  $\beta$ -MHC ratio (*H*) in CON and PRED group. Abbreviations: EDPVR: end diastolic  
1034 pressure-volume relationship; HE: Hematoxylin-Eosin; MA: Masson's trichrome; COL1:  
1035 collagen type I; COL3: collagen type III; ANP: atrial natriuretic peptide; BNP: brain  
1036 natriuretic peptide;  $\alpha$ -MHC: alpha-myosin heavy chain;  $\beta$ -MHC: beta-alpha-myosin heavy  
1037 chain. Data are means $\pm$ SEM, n=5-19 per group (\*: p<0.05).

1038 **Fig. 5. Mitochondrial morphology and function in prediabetes at week 21.** Representative  
1039 transmission electron micrographs (*A*) and number of IFM (*B*) in the left ventricle.  
1040 Magnification 12,000 $\times$ , scale bar 1  $\mu\text{m}$ . Quantification of H<sub>2</sub>O<sub>2</sub> production in SSM (*C*) and  
1041 IFM (*D*) with glutamate-malate as substrate (GM). Quantification of H<sub>2</sub>O<sub>2</sub> production in SSM  
1042 (*E*) and IFM (*F*) with succinate as substrate. Abbreviations: IFM: interfibrillar mitochondria;  
1043 SSM: subsarcolemmal mitochondria; ADP: adenosine diphosphate. Data are means $\pm$ SEM,  
1044 n=5-9 per group (\*: p<0.05).

1045 **Fig. 6. Characterization of oxidative and nitrative stress in prediabetes.** Representative  
1046 immunostaining of nitrotyrosine in the left ventricle (*A*), magnification 200 $\times$ ; scale bar 200  
1047  $\mu\text{m}$ . Representative Western blots (*B*) and quantification (*C*) of tropomyosin oxidation.  
1048 Representative Western blots (*D*) and quantification (*E*) of cardiac p66Shc expression.  
1049 Representative Western blots (*F*) and quantification of CaMKII $\delta$  (*G*) and PLB  
1050 phosphorylation on Thr<sup>17</sup> (*H*) and Ser<sup>16</sup> (*I*), and SERCA2A (*J*) expression. Abbreviations:  
1051 Tm: tropomyosin; Ox. Tm: oxidized tropomyosin; GAPDH: glyceraldehyde 3-phosphate  
1052 dehydrogenase; CaMKII $\delta$ : Ca<sup>2+</sup>/calmodulin-dependent protein kinase II; SERCA2A:  
1053 sarco/endoplasmic reticulum Ca<sup>2+</sup> ATPase II; PLB: phospholamban. Data are means $\pm$ SEM,  
1054 n=6-8 per group (\*: p<0.05).

1055 **Fig. 7. Cardiac expression of mitochondrial dynamics, autophagy/mitophagy, HSPs, and**  
1056 **apoptosis-related proteins in prediabetes.** Representative Western blots of  
1057 autophagy/mitophagy-related proteins and upstream modulators of autophagy (A),  
1058 mitochondrial fission- and fusion-related protein (B) in whole left ventricles. Representative  
1059 Western blots of mitochondrial dynamics- and mitophagy-related proteins in isolated SSM  
1060 (C) and IFM (D). Representative Western blots of HSP- (E), and apoptosis-related (F)  
1061 proteins in whole left ventricle. Abbreviations: SSM: subsarcolemmal mitochondria; IFM:  
1062 interfibrillar mitochondria; HSP: heat shock protein; GAPDH: glyceraldehyde 3-phosphate  
1063 dehydrogenase; DRP1/DLP1: dynamin-related/like protein 1; MFN2: mitofusin-2; OPA1:  
1064 optic atrophy 1; COX4: cytochrome c oxidase subunit 4, mitochondrial; LC3: 1 microtubule-  
1065 associated protein 1 light chain 3; SQSTM1/p62: sequestosome 1, BNIP3: Bcl-2/adenovirus  
1066 E1B 19 kDa protein-interacting protein 3; AMPK $\alpha$ : AMP-activated protein kinase  $\alpha$ ; GSK3 $\beta$ :  
1067 glycogen synthase kinase-3 beta.

1068 **Fig. 8. Schematic representation of the cardiac effects of prediabetes.**

1069

1070 **3. Tables**

1071 **Table 1.**

1072		CON	PRED
1073	Plasma leptin (ng/mL)	2.51 ± 0.33	5.91 ± 0.60*
1074	Plasma cholesterol (mmol/L)	1.88 ± 0.06	1.72 ± 0.08
1075	HDL cholesterol (mmol/L)	2.75 ± 0.14	2.75 ± 0.10
1076	Plasma triglyceride (mmol/L)	1.20 ± 0.10	1.31 ± 0.09
1077	LDL cholesterol (mmol/L)	0.44 ± 0.02	0.47±0.03
1078	Total Cholesterol (mmol/L)	1.61 ± 0.05	1.51 ± 0.08
1079	GOT (U/L)	82 ± 15	58 ± 4
1080	GPT (U/L)	50 ± 14	49 ± 5
1081	Uric acid (mmol/L)	24 ± 4	16 ± 1
1082	Creatinine (μmol/L)	46 ± 3	40 ± 3
1083	CRP (mg/L)	109.56 ± 1.24	94.96 ± 3.87*
1084			

1085

1086

1087 **Table 2.**

1088

CON      PRED

1089 LV mass (g)

$1.01 \pm 0.04$      $1.22 \pm 0.07^*$

1090 LVAWTd (mm)

$1.89 \pm 0.12$      $2.07 \pm 0.12$

1091 LVAWTs (mm)

$2.86 \pm 0.17$      $3.42 \pm 0.11^*$

1092 LVPWTd (mm)

$1.86 \pm 0.07$      $2.05 \pm 0.04^*$

1093 LVPWTs (mm)

$2.72 \pm 0.12$      $3.25 \pm 0.15^*$

1094 LVEDD (mm)

$7.71 \pm 0.22$      $7.75 \pm 0.17$

1095 LVESD (mm)

$4.93 \pm 0.22$      $4.96 \pm 0.31$

1096 FS (%)

$36.0 \pm 2.2$        $37.4 \pm 3.8$

1097 HR (1/min)

$335 \pm 13$          $348 \pm 10$

1098

1099

1100 **Table 3.**

1101		CON	PRED
1102	MAP (mmHg)	110.1 ± 7.3	113.6 ± 6.1
1103	LVESP (mmHg)	116.6 ± 5.6	120.0 ± 6.8
1104	LVEDP (mmHg)	4.4 ± 0.4	4.0 ± 0.2
1105	LVEDV (μL)	292.8 ± 14.5	280.2 ± 9.6
1106	LVESV (μL)	130.7 ± 6.9	127.5 ± 4.5
1107	SV (μl)	162.1 ± 9.1	152.8 ± 7.7
1108	CO (mL/min)	59.5 ± 3.2	56.6 ± 2.3
1109	EF (%)	55.3 ± 1.3	54.4 ± 1.3
1110	SW (mmHg·mL)	14.5 ± 0.5	13.6 ± 0.6
1111	dP/dtmax (mmHg/s)	7226 ± 487	7387 ± 401
1112	dP/dtmin (mmHg/s)	-8198 ± 680	-8551 ± 545
1113	τ (Glantz) (ms)	12.6 ± 0.3	12.1 ± 0.4
1114	TPR [(mmHg·min)/mL]	1.90 ± 0.19	2.00 ± 0.12
1115	Slope of ESPVR (mmHg/μL)	2.68 ± 0.12	2.71 ± 0.06
1116	Slope of EDPVR (mmHg/μL)	0.026 ± 0.001	0.037 ± 0.004*
1117	PRSW (mmHg)	100.5 ± 5.2	98.9 ± 4.1

1118	Slope of dP/dtmax-EDV [(mmHg/s)/ $\mu$ L]	$34.3 \pm 2.3$	$35.2 \pm 2.2$
1119	Maximal power (mW)	$91.8 \pm 8.2$	$98.2 \pm 12.5$
1120			

1121

1122 **Table 4.**

1123

CON

PRED

1124 Citrate-synthase activity (U/mg protein)

223.12 ± 9.98 220.44 ± 8.32

1125 NADH:Ubiquinone-Oxidoreductase activity (U/mg protein)

40.52 ± 2.55 36.48 ± 2.99

1126 NADH:Cytochrome c- Oxidoreductase activity (U/mg protein)

7.85 ± 1.18 8.47 ± 1.31

1127 Succinate:Cytochrome-c-Oxidoreductase activity (U/mg protein)

21.09 ± 1.49 23.57 ± 1.61

1128 Succinate-Dehydrogenase activity (U/mg protein)

84.06 ± 5.83 80.09 ± 3.42

1129 Cytochrome-c-Oxidase activity (U/mg protein)

38.74 ± 3.15 40.36 ± 2.33

1130 **Table 5.**

1131	CON	PRED	CON	PRED	
1132	Subsarcolemmal	Subsarcolemmal	Interfibrillar	Interfibrillar	
1133	(pmol/mL×sec)	(pmol/mL×sec)	(pmol/mL×sec)	(pmol/mL×sec)	
1134	Glutamate-malate	25.08 ± 3.6	21.06 ± 3.53	58.6 ± 19.31	61.78 ± 21.41
1135	ADP	203.31 ± 32.57	194.03 ± 42.16	304.23 ± 25.75	287.9 ± 22.35
1136	Cytochrome c	260.8 ± 28.27	287.06 ± 54.91	335.96 ± 25.79	345.41 ± 28.17
1137	Succinate	306.2 ± 25.19	289.74 ± 23.23	367.76 ± 15.74	393.56 ± 18.82
1138	Rotenone	143.12 ± 18.19	139.7 ± 23.64	238.4 ± 18.44	220.73 ± 16.19
1139	CAT	105.95 ± 8.89	106.5 ± 12.22	159.78 ± 6.86	156.6 ± 8.03

1140



1142 **Table 6.**

1143	Total LV	CON	PRED
1144	BNIP3/GAPDH ratio	0.59 ± 0.03	0.44 ± 0.02*
1145	MFN2/GAPDH ratio	0.27 ± 0.01	0.36 ± 0.02*
1146	OPA1/GAPDH ratio	1.47 ± 0.11	1.63 ± 0.1
1147	DRP1/GAPDH ratio	1.16 ± 0.08	1.34 ± 0.14
1148	LC3-II/GAPDH ratio	0.56 ± 0.07	0.56 ± 0.05
1149	p62/GAPDH ratio	3.05 ± 0.18	3.45 ± 0.23
1150	Parkin/GAPDH ratio	2.25 ± 0.14	2.43 ± 0.17
1151	Beclin1/GAPDH ratio	0.81 ± 0.07	0.82 ± 0.07
1152	Phospho AKT(Ser <sup>473</sup> )/AKT ratio	0.32 ± 0.04	0.29 ± 0.02
1153	Phospho AMPK(Thr <sup>172</sup> )/AMPK ratio	0.12 ± 0.02	0.21 ± 0.06
1154	Phospho S6(Ser <sup>235/236</sup> )/S6 ratio	2.62 ± 1.08	2.16 ± 0.61
1155	Phospho GSK3β(Ser <sup>9</sup> )/GSK3β ratio	0.8 ± 0.09	0.72 ± 0.1
1156	Bcl-2/GAPDH ratio	0.23 ± 0.01	0.20 ± 0.003*
1157	Bcl-2/Bax ratio	0.15 ± 0.02	0.15 ± 0.02
1158	caspase-3/GAPDH ratio	0.05 ± 0.001	0.04 ± 0.003
1159	P-HSP-27(Ser <sup>82</sup> )/T-HSP-27 ratio	0.34 ± 0.05	0.28 ± 0.02
1160	HSP-60/GAPDH ratio	0.85 ± 0.02	0.84 ± 0.02
1161	HSP-70/GAPDH ratio	0.53 ± 0.01	0.51 ± 0.01
1162	HSP-90/GAPDH ratio	0.46 ± 0.01	0.50 ± 0.02

1163

1164			
1165	Subsarcolemmal mitochondria	CON	PRED
1166	OPA1/COX4 ratio	1.34 ± 0.07	1.32 ± 0.06
1167	LC3-II/COX4 ratio	0.22 ± 0.1	0.25 ± 0.04
1168	p62/COX4 ratio	0.13 ± 0.02	0.12 ± 0.03
1169	Interfibrillar mitochondria	CON	PRED
1170	OPA1/COX4 ratio	1.44 ± 0.15	1.52 ± 0.14
1171	LC3-II/COX4 ratio	0.22 ± 0.09	0.29 ± 0.07
1172	p62/COX4 ratio	0.35 ± 0.06	0.36 ± 0.04
1173			

1174

#### 1175 **4. Table legends**

1176 **Table 1. Plasma parameters at week 21.** Data are means±SEM for 12 rat per group (\*:  
1177 p<0.05).

1178 **Table 2. Characterization of cardiac morphology and function in prediabetes by means**  
1179 **of echocardiography.** Abbreviations: LV mass: Left Ventricular Mass; LVAWTs: Left  
1180 Ventricular Anterior Wall Thickness, diastolic; LVAWTs: Left Ventricular Anterior Wall  
1181 Thickness, systolic; LVPWTs: Left Ventricular Posterior Wall Thickness, systolic; LVPWTd:  
1182 Left Ventricular Posterior Wall Thickness, diastolic; FS%: Fractional Shortening %; HR:  
1183 Heart rate. Data are means±SEM for 10 rat per group (\*: p<0.05).

1184 **Table 3. Characterization of left ventricular (LV) hemodynamics in vivo in prediabetes**  
1185 **by means of pressure-volume analysis.** Abbreviations: MAP: Mean Arterial Pressure;  
1186 LVESP: Left Ventricular End-Systolic Pressure; LVEDP: Left Ventricular End-Diastolic  
1187 Pressure; LVESV: Left Ventricular End-Systolic Volume; LVEDV: Left Ventricular End-  
1188 Diastolic Volume; SV: Stroke Volume; CO: Cardiac Output; EF: Ejection Fraction; SW:  
1189 Stroke Work; dP/dtmax: maximal slope of LV systolic pressure increment; dP/dtmin:  
1190 maximal slope of LV diastolic pressure decrement;  $\tau$ : time constant of LV pressure decay;  
1191 TPR: Total Peripheral Resistance; ESPVR: End-Systolic Pressure-Volume Relationship;  
1192 EDPVR: End-Diastolic Pressure-Volume Relationship; PRSW: Preload Recrutable Stroke  
1193 Work; dP/dtmax-EDV: the slope of the dP/dtmax-end-diastolic volume relationship. Data are  
1194 means±SEM for 10 rat per group (\*: p<0.05).

1195 **Table 4. Quantification of cardiac mitochondria enzyme activity in left ventricle.** Data  
1196 are means±SEM for 5-9 rat per group (\*: p<0.05).

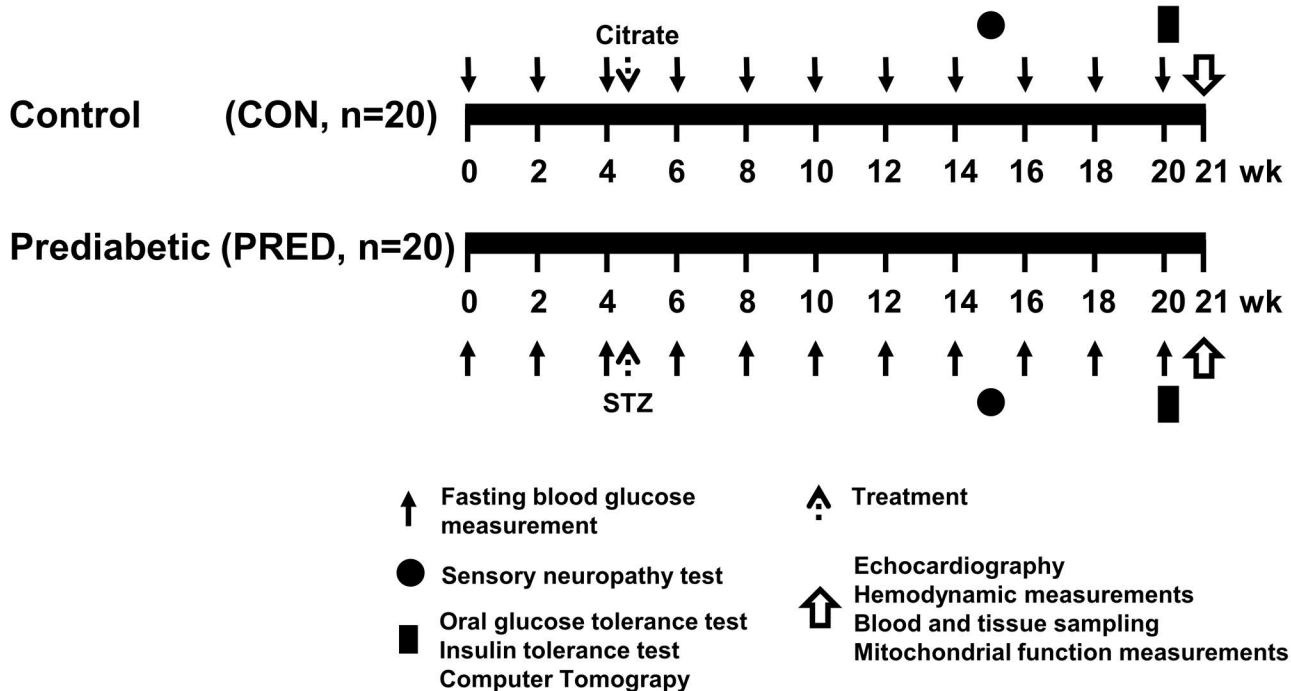
1197 **Table 5. Quantification of mitochondrial oxygen consumption.** Abbreviations: ADP:  
1198 adenosine diphosphate. CAT: carboxyatractyloside. Data are means±SEM for 9 rat per group  
1199 (\*: p<0.05).

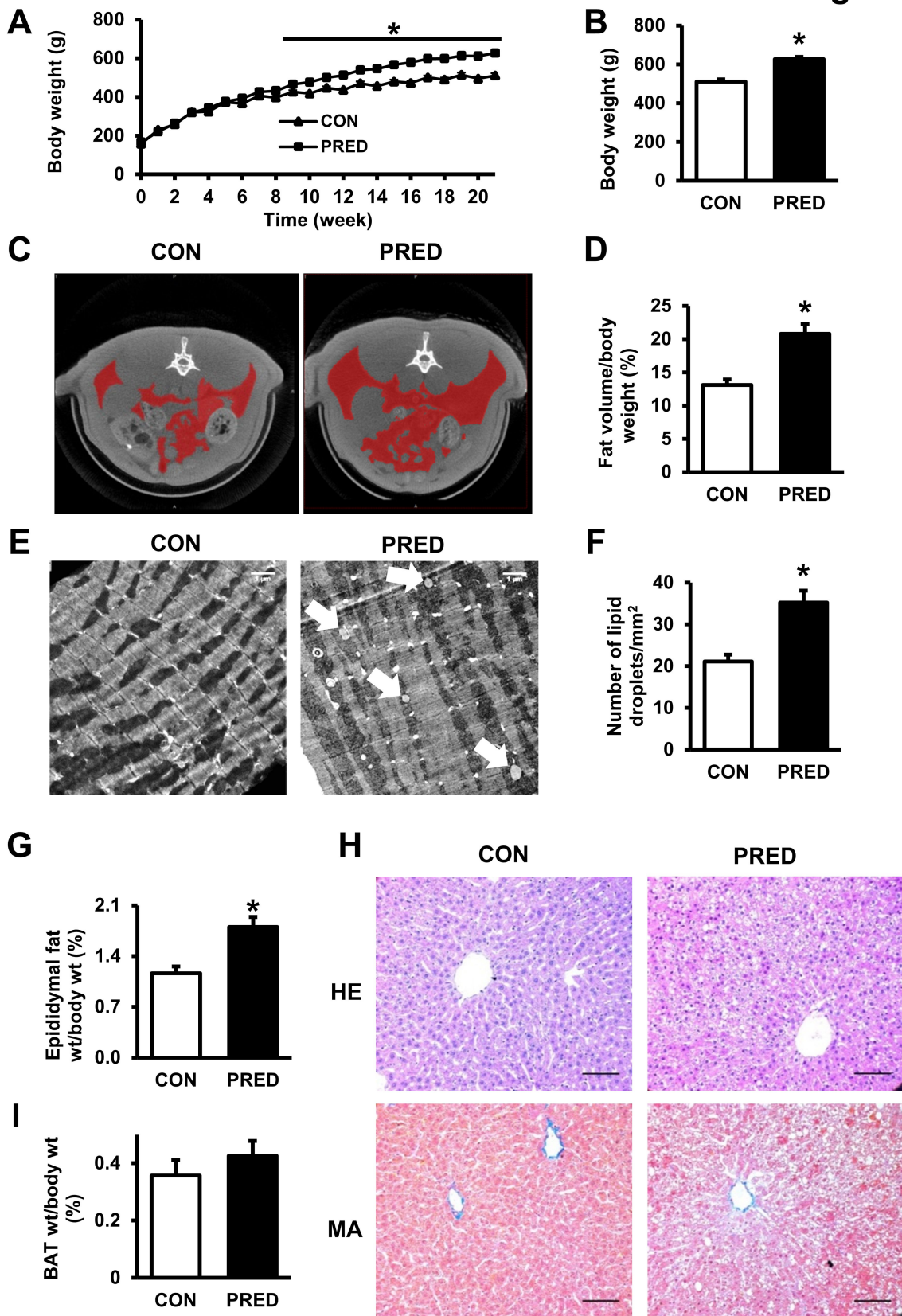
1200 **Table 6. Quantification of HSPs, apoptosis, mitochondrial dynamics- and mitophagy-**  
1201 **related protein expressions in isolated mitochondrial fractions and whole left ventricles.**

1202 Data are means±SEM for 8 rat per group (\*: p<0.05).

1203

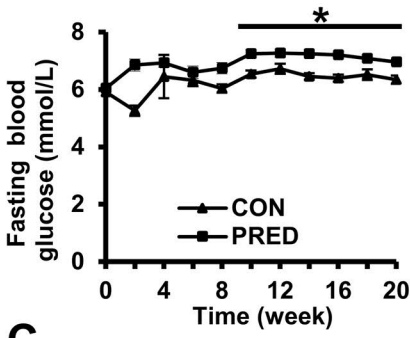
# Figure 1



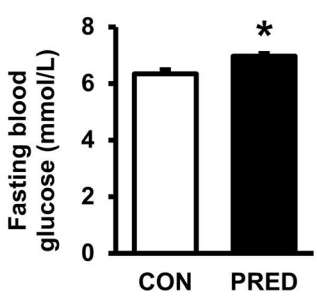
**Figure 2**

# Figure 3

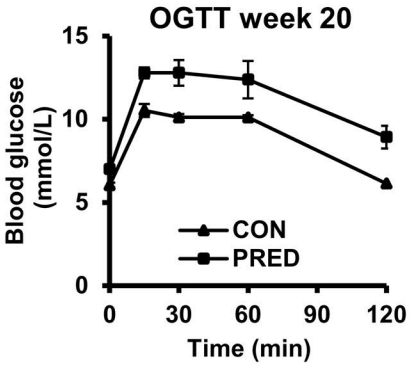
**A**



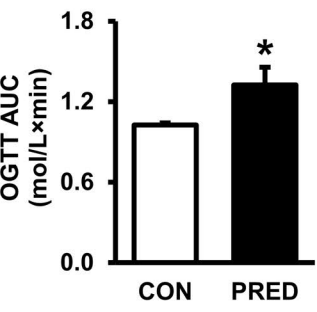
**B**



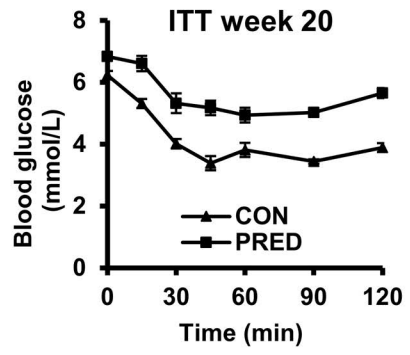
**C**



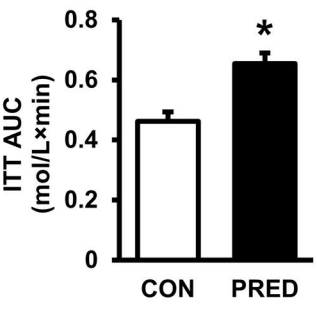
**D**



**E**



**F**



**G**

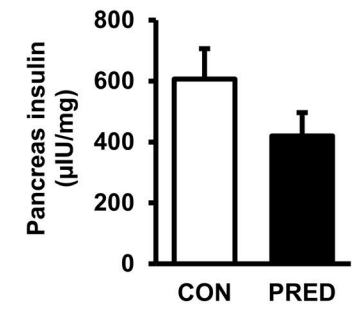


# Figure 4

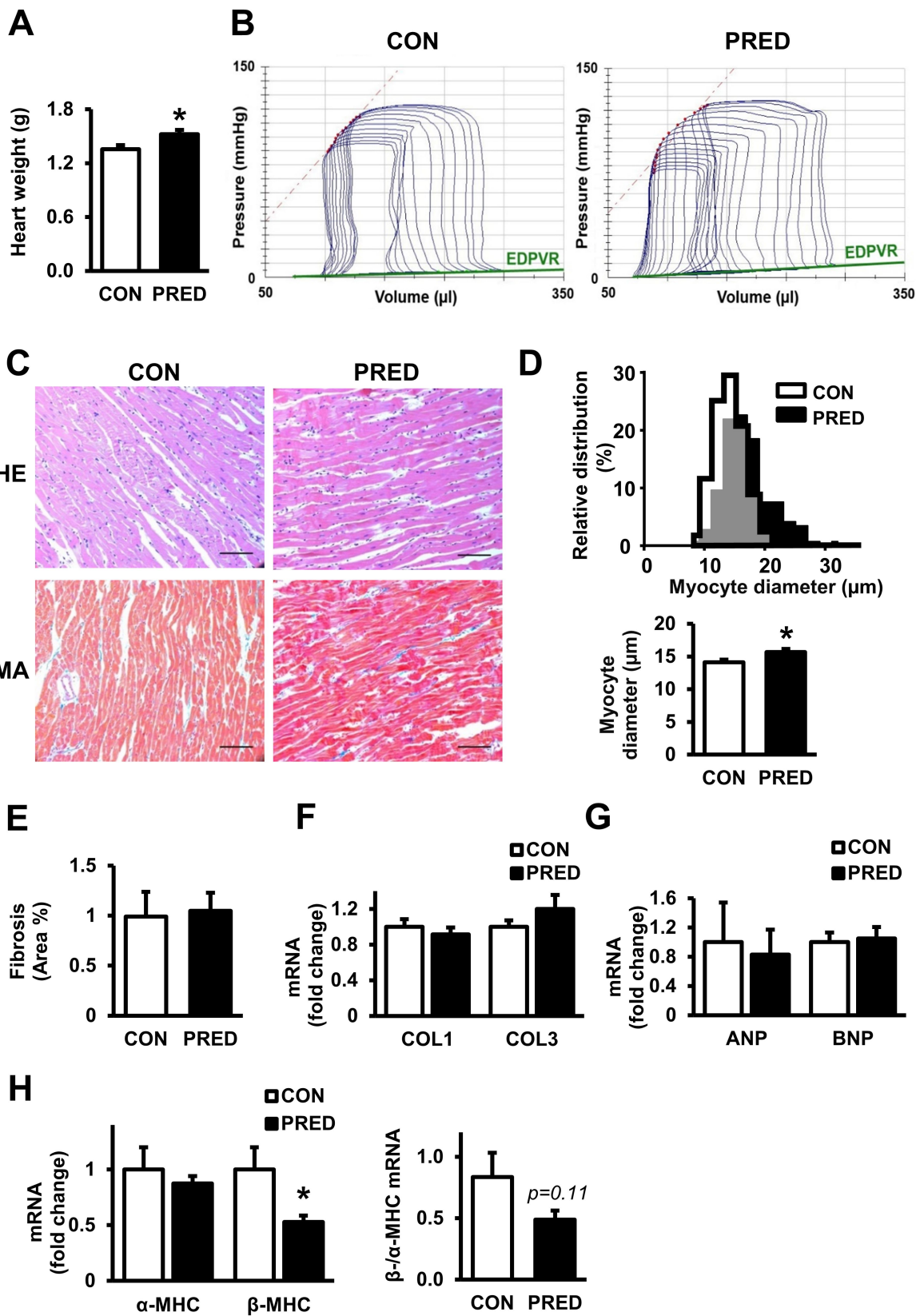
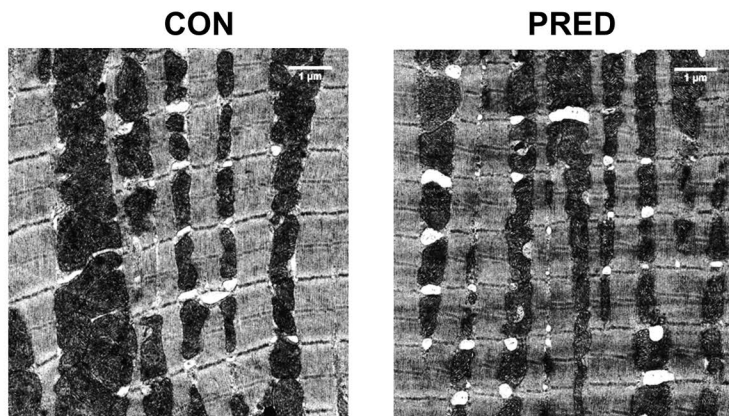
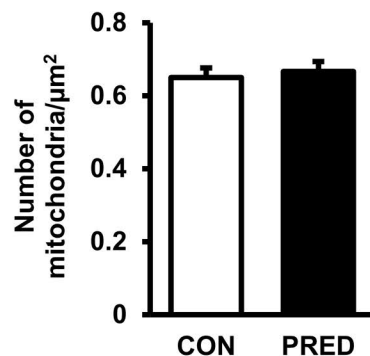


# Figure 5

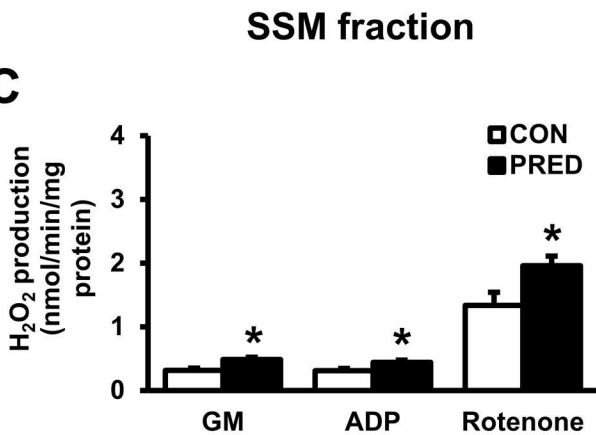
## A



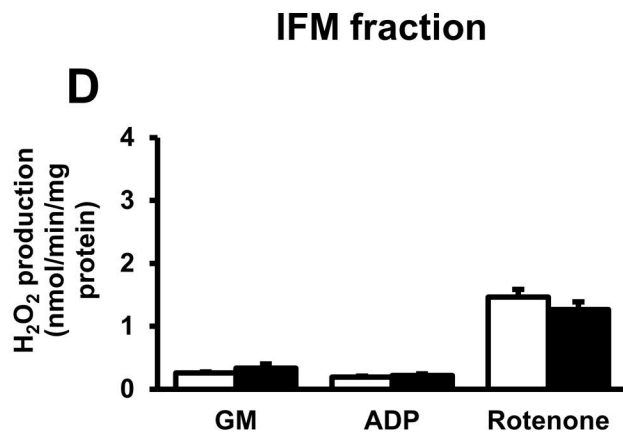
## B



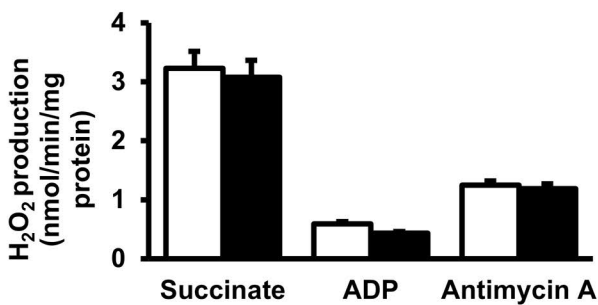
## C



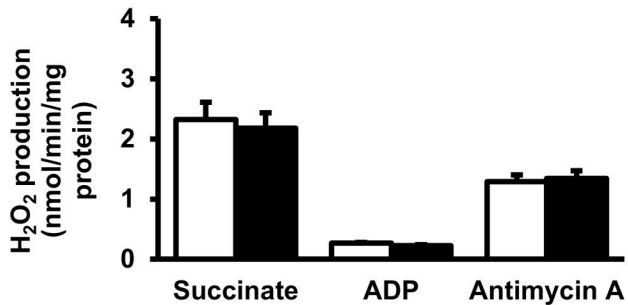
## D



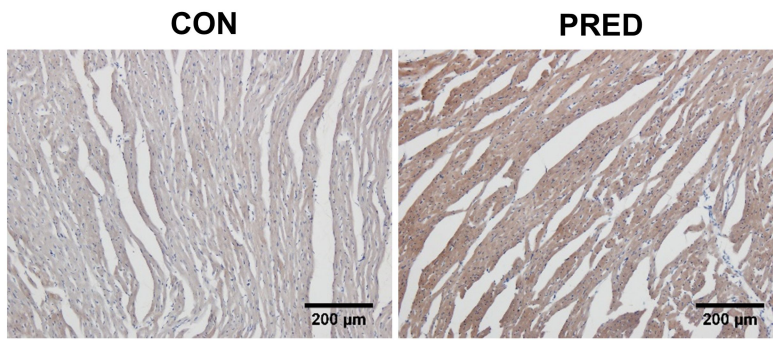
## E



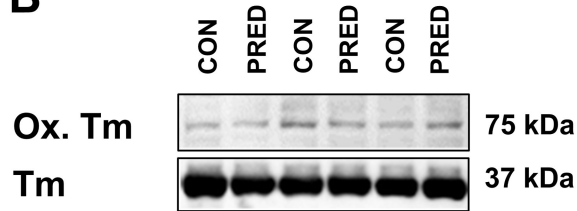
## F



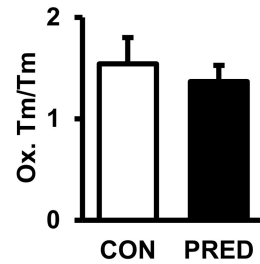
**A**



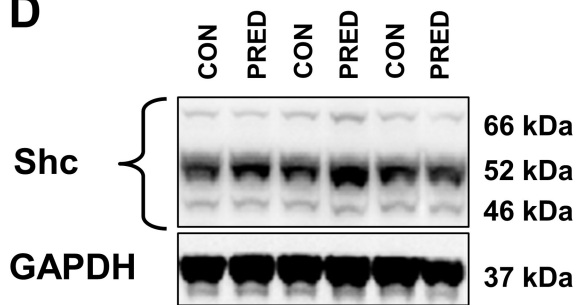
**B**



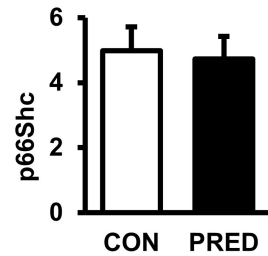
**C**



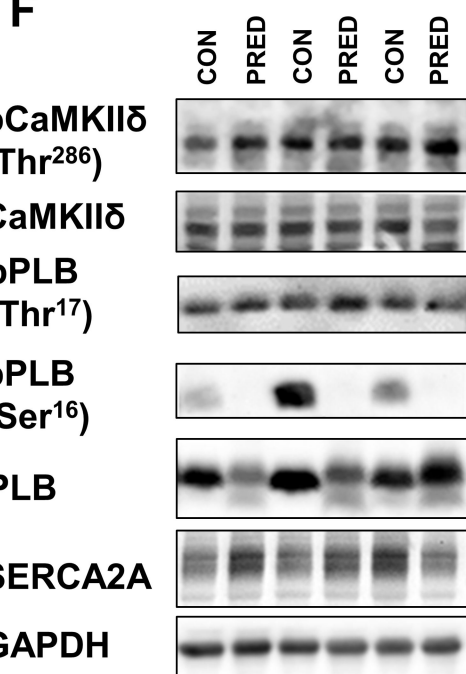
**D**



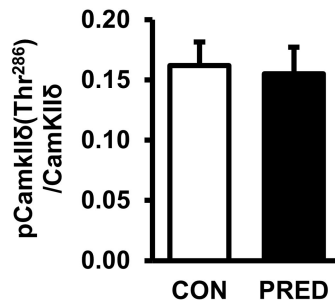
**E**



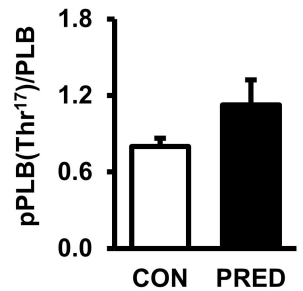
**F**



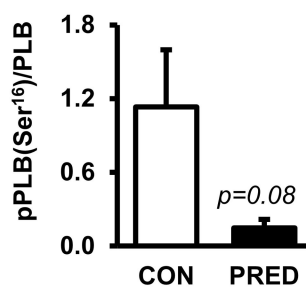
**G**



**H**



**I**



**J**

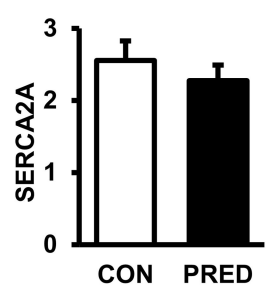


**Figure 7**

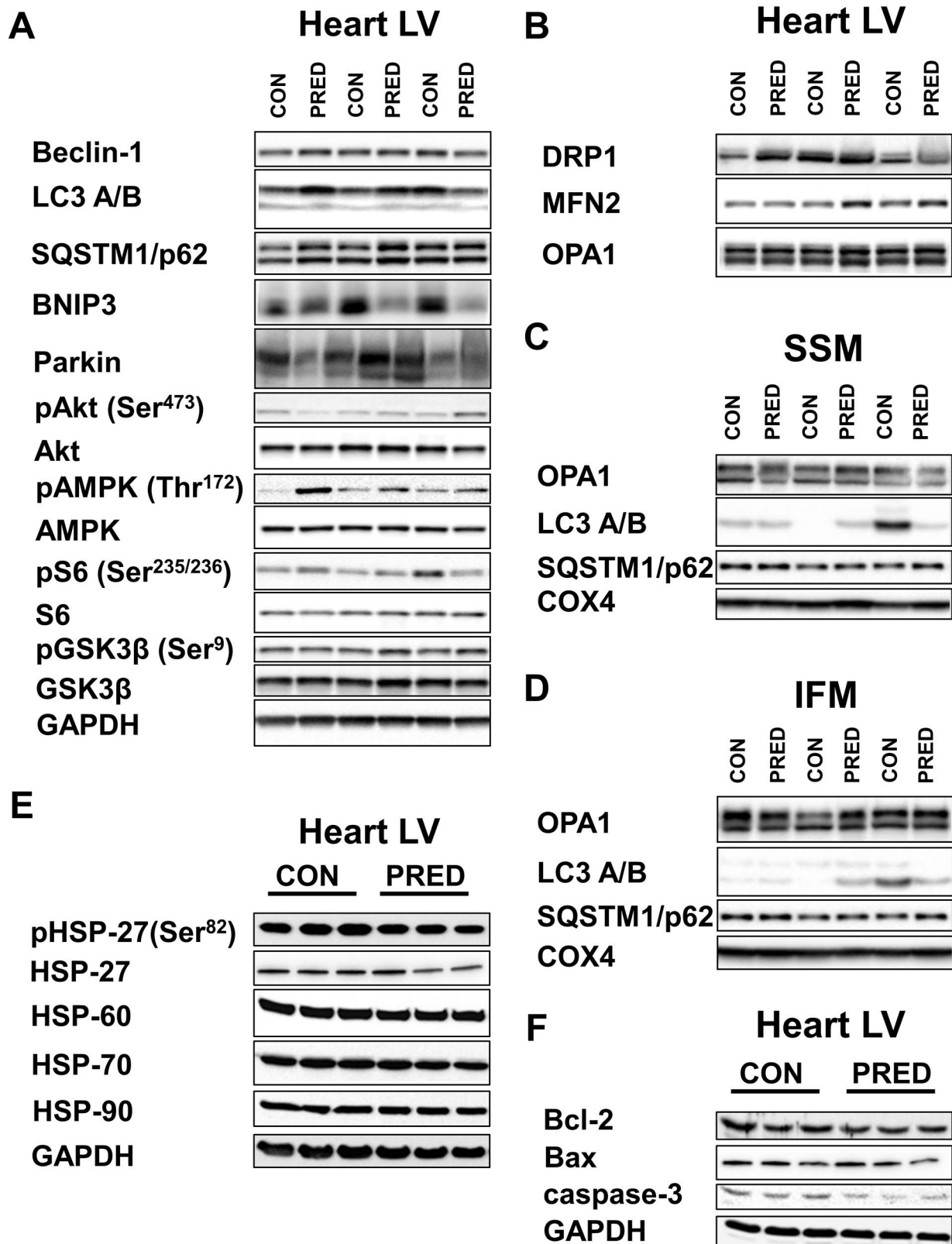


**Figure 8**

